

Multiaxial fatigue criteria for offshore mooring
chain links subjected to out-of-plane bending
MSc Thesis

Ingmar Calf

August 21, 2015

1. Abstract

The out-of-plane bending of offshore mooring chains leads to a rapid deterioration of the chain, ultimately leading to failure in a period that is a fraction of the design-life. The deformation of the contact surface of the chainlinks leads to the interlocking of the link. This in turn causes the chain to behave like a bending beam. The combination of the chains behaving in this manner and the vessel movement leads to a bending moment in the chain link, especially in the top section, where the tensions are high. Due to the alternating nature of the loading, multiaxial fatigue effects cause chain failure.

In this thesis, a literature study is performed, forming an introduction to the general concept of fatigue and the exploration of available methods. For multiaxial loadings, so-called critical plane methods are widely accepted as the most effective approach. This critical plane method search for the material plane experiencing most damage, according to the damage criterion that is assessed. Furthermore, a number of methods for the cycle decomposition are present. For uniaxial methods, the rainflow method is most used. Applying this method to multiaxial fatigue problems can lead to problems, which leads to the formation of alternative approaches. The other approaches being discussed are the Wang & Brown method and the Modified Wang & Brown method. The Bannantine & Socie method is discussed too, but could be classified as a critical plane search algorithm, instead of a novel cycle counting method.

After the exploration of the problem, a finite element model is created. This model consists of multiple chain links, that are proofloaded while plastic deformation is allowed. This leads to the aforementioned deformation of the contact surfaces on the links. After the proofloading step is completed, three different cases are performed with an elastic material formulation. These cases comprise of varying angle ranges; Case 1 only induces an out-of-plane bending in the analysed link, Case 2 induces an out-of-plane and in-plane load, while Case 3 is similar to Case 2, apart from an added phase difference between the two angles. The stress and strain results from the finite element analyses are input in the Pragtic fatigue software. For each case, a number of fatigue criteria are calculated. These criteria are, named after the author, the following: McDiarmid, Dang Van, Matake, Liu & Mahadevan, Carpinteri & Spagnoli, Findley, Wang & Brown & Miller, Smith & Watson & Topper and Socie. Different critical plane search algorithms and/or cycle counting methods have been explored. Some of these criteria lead to a Fatigue Index, while others lead to an Accumulated Damage formulation.

From the results it is clear that the cases combining two angles lead to higher damages, leading to the believe that the multiaxial behaviour should be taken into account when assessing fatigue damage of mooring chains. Furthermore, it seems that for the different cases, the SWT criterion gives either the highest or the lowest damage. As this is originally a multiaxial parameter, it shows that the use of traditional uniaxial methods could either over- or underestimate the damage, depending on the specific loading. Furthermore, results show that the criterion that is suggested by Bureau Veritas' Guidance Note on OPB, namely the Dang Van criterion, often gives the lowest fatigue index. This suggests that this criterion might not be conservative enough. This statement needs to be validated with the help of experiments. Furthermore, the method specifically aimed

at multiaxial problems, the Wang & Brown method (including the multiaxial cycle counting method), leads to highest accumulated damage. As this method was aimed for multiaxial and non-proportional loading, it can be reasoned that this method makes a conservative, proper prediction. As for the critical plane orientation, it seems that the most damaging plane, likely the location of crack growth, is often close to the shear plane. This fuels the believe that the shear stress is the factor driving the OPB failure mode. However, since this problem inherently involves a mean stress (the tension on the mooring chain), the critical plane does not need to be the shear plane. When exploring this with the globe plane search algorithm, it seems that the critical plane is often a plane oriented at some angle in between the shear and normal plane.

The results and statements made in this report are at this point mathematical. As the OPB concept is relatively newly discovered, more experiments are needed to be able to back up any statements that can be made. Furthermore, the research presented here could benefit from a larger group of cases, and added detail on the loading part of the analyses. Furthermore, as material fatigue parameters are limited, a sensitivity anayses on these parameters could shed some light on the influence of parameters used. The parameters used in this report are taken from similar materials and should at least give a very reasonable approximation of the material's fatigue behaviour.

Contents

| | | |
|----------|--|-----------|
| 1 | Abstract | 1 |
| 2 | Acknowledgments | 5 |
| 3 | Introduction | 6 |
| 4 | Literature review | 7 |
| 4.1 | Multiaxial Fatigue | 7 |
| 4.1.1 | Fatigue | 7 |
| 4.1.2 | Cycle counting | 13 |
| 4.1.3 | Criteria | 22 |
| 4.2 | Mooring chain link | 31 |
| 4.2.1 | Mooring systems | 31 |
| 4.2.2 | Out-of-plane bending | 32 |
| 5 | Problem statement | 34 |
| 5.1 | OPB Problem | 34 |
| 5.2 | Solution method | 34 |
| 5.2.1 | Software | 35 |
| 6 | FE Analysis | 36 |
| 6.1 | Finite Element Analysis | 36 |
| 6.1.1 | Finite Elements | 36 |
| 6.1.2 | Boundary Conditions | 37 |
| 6.2 | FE Chain link model | 37 |
| 6.2.1 | Geometry & Material | 37 |
| 6.2.2 | FE: Loads, constraints & mesh | 39 |
| 6.2.3 | Limitations | 46 |
| 6.3 | Analysis results | 47 |
| 6.3.1 | Deformation, stresses & strain | 47 |
| 7 | Fatigue Analysis | 54 |
| 7.1 | Critical plane criterion | 54 |
| 7.1.1 | Bannantine & Socie | 54 |
| 7.1.2 | Globe approach | 54 |
| 7.2 | Fatigue calculations | 55 |
| 7.2.1 | Fatigue Index | 56 |
| 7.2.2 | Fatigue damage | 59 |
| 7.2.3 | Globe concept | 65 |

| | | |
|----------|---|-----------|
| 8 | Conclusions | 70 |
| 9 | Discussion & Recommendations | 71 |
| | Appendices | 72 |
| A | Crack Locations | 73 |
| B | Pragtic | 74 |
| C | Stress Time History Case 3 L3-L4 | 85 |

2. Acknowledgments

I would like to express my gratitude to everybody that helped me conducting this thesis, and finalizing my education at TU Delft. Specifically, I would like to thank Arie Romeijn, for guiding me in the process of writing this thesis. At times, everything I had done so far seemed utterly useless, but luckily Arie reassured me everything was not hopeless.

I owe a great deal of gratitude to LMC, who let me return each day without me delivering much tangible results, except the vague promise of fatigue calculations.

Also, ir. Jan Papuga, developer of the Pragtic fatigue software deserves gratitude, for helping me figure out programming errors and mistakes. The amount of e-mails and attachments sent back and forth is quite significant, so mr. Papuga's effort is undeniable.

Furthermore, I would like to thank my parents for patiently supporting me during 7 years at TU Delft.

And finally I would like to thank my girlfriend Ida, for letting me spoil many dinners with talk about mooring chain bending, or being irritable due to computer models that would not do what I wanted them to do.

3. Introduction

This report contains the proceedings of the MSc thesis of Ingmar Calf. This thesis is conducted to be able to obtain the Master of Science degree in Marine Technology at Delft University of Technology. The specialization of the followed master's programme is the structural science track, *ship & offshore structures*. The research was supervised by dr. A. Romeijn and professor M. Kaminski. The thesis was conducted on location at London Marine Consultants, London. This company specializes in turret mooring systems and as such was interested in gaining more knowledge of the OPB phenomenon.

The main subject of the research is the multiaxial fatigue prediction of offshore mooring chains due to out-of-plane bending. The out-of-plane bending significantly deteriorates the mooring chains, leading to chain failure and as a result in possible accidents, which can cause oil spills or loss of material and/or life. Therefore, one would like to be able to predict the failure of a mooring chain due to this phenomena. It is then possible to improve the design of the mooring system, to prevent failure within the life-span of the chains. The goal of this report is exploring the different possible multiaxial fatigue criteria that may be employed to calculate the life-time. This will hopefully provide some theoretical background for subsequent research projects, or some guidance for, e.g., classification societies. The report build up as follows. First a general theoretical exploration of the subject is presented. This will focus on various fatigue related subjects to have a proper understanding of concepts. Not only will this elaborate on general concepts, but also more in-detail on later employed theories and methods. Furthermore, it will give some background information on the problem of out-of-plane bending of mooring chains. After that, the problem is briefly stated. In the subsequent chapter the finite element model that is used to perform analysis is presented. The loads applied to the model, meant to mimic real-life loading is presented as well. Finally, the results of the FE analysis will be presented. Then, with these results fatigue calculation will be performed, which will be presented in chapter 7. The results for all the different approaches will be discussed there. Finally, some recommendations will be done in chapter 9.

4. Literature review

4.1 Multiaxial Fatigue

This chapter is aimed at introducing some basic fatigue terminology and discussing relevant literature on the subject. The chapter is divided by subject or concept, but sometimes terms are used which have not been properly introduced yet. As many subjects in this field are interdependent, this is more or less inevitable. A general introduction to fatigue analysis is given in Section 4.1.1. In this section a very brief overview of developments is given, while basic terminology and concepts are introduced. Even though cycle counting is already briefly mentioned in this section, it is such a fundamental part of fatigue analysis that the details for multiaxial fatigue are discussed in the subsequent section 4.1.2. An overview of different fatigue criteria is given in Section 4.1.3. Here the different types of fatigue criteria are discussed with respect to their formulation, applicability, advantages and shortcomings. This chapter concludes by linking the fatigue theory to the specific problem of mooring chains, used for offshore mooring applications, in Section 4.2

4.1.1 Fatigue

The aim of this section is to present some of the relevant theory and backgrounds of the fatigue phenomenon, to develop a basic understanding. Over the years the subject has experienced a great deal of attention, resulting in a vast amount of literature. However, when one goes through the wide range of conference papers, thesis reports and research papers, it becomes clear that there is still a lot about the subject that is unknown.

This section is split up in a number of sections, each aiming at a certain part of the theory. Firstly, focus is put on some general definitions and terms. As this thesis deals with multiaxial fatigue, while much literature is on uniaxial stress states, the differences between the two will be expanded on in the next section. Finally, the different types of loading associated with fatigue damage will be discussed.

4.1.1.1 General

4.1.1.1.1 S-N Approach As mentioned before, the vast amount of research makes it impossible to write a full comprehensible historical overview of fatigue research. The aim of this chapter is by no means intended as giving such an overview, but rather to introduce some of the main concepts.

The fatigue phenomenon is defined by the accumulation of damage, due to a cyclic application of stresses. The material may fail eventually, even though the stress has never exceeded the maximum yield strength or the ultimate limit stress of the material. This failure mode has received attention for more than 150 years, to a greater or lesser extent. One of the first papers on fatigue was by J. Rankine, on the fatigue of railway axles, following a train accident. Already then, he recognized that " the unexpected fracture of originally good axles, after running for several years without any appearance of unsoundness, must be caused by a gradual deterioration in the course of working..." [Rankine, 1842].

A. Wöhler (1819-1914) spend a great deal of time working on railway axle fatigue, leading to the so-called *Wöhler-* or *S-N-curves*. These systematic curves give the cyclic stress range versus the number of load cycles on a logarithmic scale. S-N-curves are an empirical way to estimate fatigue behaviour of components, as these curves are constructed by means of test data. The S-N curve defines an *endurance limit*. If the applied stress is below this limit, the material has *infinite life*, in other words: the material will not fail. Many S-N curves have been developed for many different details, geometries and applications, as they provide an easy and quick way to assess the fatigue damage of structural components. S-N-curves are often used in combination with the *Palmgren-Miner Rule*, to account for the damage accumulation in the material. The Palmgren-Miner Rule is a rule that basically assumes a linear relation between the number of cycles in a certain stress range and the fatigue life that is consumed. It is formulated in Equation 4.1.

$$D = \sum_{i=1}^k \frac{n_i}{N} = \sum_{i=1}^k D^{(i)} \quad (4.1)$$

The Palmgren-Miner rule states that failure occurs if $D = 1$. The Palmgren-Miner damage accumulation rule assumes that the order of the applied cycles does not influence the total damage. This relationship is not the only option to calculate the total damage, there are a number of non-linear damage accumulation hypotheses [Mikhailov et al.,2001]. The Serensen-Kogaev (sometimes referred to as Serensen-Kogayev) is presented here in accordance with [Karolczuk and Macha, NOWN]. This relationship was proposed to get a better agreement with a loading that is non-regular in time [Mikhailov and Namestnikova, 2001].

$$D = \frac{1}{p} \sum_{i=1}^k D^{(i)},$$

$$p = \frac{\sum_{i=1}^k F_{eq,a}^{(i)} f^{(i)} - aF_{af}}{F_{eq,a}^{max} - aF_{af}} \quad (4.2)$$

$$f^{(i)} = \frac{n^i}{\sum_i n^{(i)}}$$

The factor p is sometimes called the *Serensen-Kogayev coefficient*. It is easy to see that when $p = 1$ the Palmgren-Miner rule of 4.1 results. In Equation 4.2, $f^{(i)}$ is the frequency of the i -th loading level; the number of cycles at a particular loading level divided by the total number of cycles. $F_{eq,a}^{max}$ is the maximum amplitude of the generalised fatigue damage parameter (which e.g. can be shear stress, normal stress or strain; τ , σ or γ respectively). Furthermore, k is the number of class intervals of the damage parameter; e.g. the number of stress ranges.

Other damage accumulation hypotheses have been developed, for instance *Ro-billard & Cailletaud*, but according to [Socie and Marquis, 2000] these are very complex and require a lot of material constants (and hence a lot of experiments to determine these constants). Therefore, these have been omitted from this introduction.

Finally, the fatigue life can be calculated by means of Equation 4.3,

$$T = \frac{T_0}{D(T_0)} \quad (4.3)$$

For regimes where plastic deformation plays an important role, it can be useful to look at the strains instead of the stresses. This approach can be described by the famous *Manson & Coffin* relationship, which is given as:

$$\frac{\Delta\varepsilon_{pl}}{2} = \varepsilon'_f (2N)^c \quad (4.4)$$

In Equation 4.4, $\frac{\Delta\varepsilon_{pl}}{2}$ is the plastic strain amplitude, ε'_f is an empirical constant called *fatigue ductility coefficient*, c is another empirical constant called *fatigue ductility exponent* and N is the number of cycles to failure ($2N$ being the number of reversals).

4.1.1.1.2 Fracture Mechanics Fatigue analyses implementing the standardised S-N-curve approach make use of the location of the endurance limit; infinite life is assumed below the limit, while fatigue damage occurs above the limit. However, a material may have a significant life even when stress ranges higher than the endurance limit are applied. Therefore it is useful to be able to predict the remaining fatigue life when the endurance limit is indeed exceeded. The term *damage tolerance* aptly describes the foundation of the approach. Development of the approach described above came into life with *Fracture Mechanics*, which investigates the crack propagation behaviour in materials on a micro-structural level. Again, this section is not meant as a complete historic or theoretic overview of all developments in this field. However, a general introduction to fatigue would not be complete without mentioning some of the accomplishments of Fracture Mechanics.

In 1903, Ewing & Humfrey optically examined specimens during different stages of the fatigue life [Socie and Marquis, 2000]. During their research they observed the basis of *crack nucleation* and *crack growth*.

One of the first people to investigate these phenomena was A.A. Griffith, who realized crack propagation must be a contributor, as polished test samples demonstrated an increased fatigue resistance [Griffith, 1920].

These two phenomena are at the basis of fracture mechanics, with the main distinction being between nucleation and growth. This distinction is quite crude as more stages are usually defined. To look at crack nucleation, one has to go down to the micro-structural level, i.e. the crystal lattice of the metal or the grains in the metal. The cyclic loading of a material may result in the formation of slip-bands, which occur due to the movement of dislocations in the micro-structure. The dislocations may exist in the material due to precipitates, inclusions and/or impurities. When the dislocation start to move, the cyclic stresses may exceed a certain threshold value, which can then result in plastic deformation. If this repeatedly happens, a *slip-band* comes into existence. When slip-bands keep undergoing plastic strain, the result is the formation of a small crack. An important factor in this is the grain size, as smaller grains make it harder for dislocations to move along the material (basically, the grain boundaries can arrest the dislocation movement). Furthermore, it is good to realize that cracks usually nucleate at the material surface.

Before getting into some more fracture mechanics, some terminology has to be discussed. This terminology is in accordance with [Socie and Marquis, 2000], but is universally applied in the fracture mechanics field. The terminology describes certain loading mechanisms and crack growth stages, which enables one to quickly distinguish different general cases in more detailed stages of fracture mechanics. First of all, the way in which a crack is loaded is distinguished. These are the so-called *modes of loading*, being Mode I, Mode II and Mode III. Mode I is used to describe the case in which the load tends to *open* the crack. Mode II is used to describe a load that is *in-plane shear*. Mode III is also a shear load, but this time it works *out-of-plane*. Now the crack loading is covered, but the *stages* of growth still need addressing. First of all, the growth stages are distinguished as Stage I and Stage II. This is important to describe how cracks grow into the surface of the material. As one could imagine, not only the size of a crack on the surface of a material is important, but the depth to which a crack extends *into* the material might be even more important. Depending on the material, a crack may propagate into the material along the maximum shear stress planes. The plastic deformation in the slip bands is a shear stress process, which is why cracks usually initiate along the maximum shear stress plane. In fact, the stress at which slip-bands are initiated is a material property, called *maximum resolved shear stress*. The propagation along these planes is defined as *Stage I growth*. At some point, the crack has grown sufficiently large, after which the propagation direction will be perpendicular to the applied (tensile) stress. To fully describe the crack growth, the fact that shear cracks can grow in two different ways needs to be addressed. Therefore the distinction between *Case A* and *Case B* is added. For a *Case A* crack, the shear stress acts on the surface of the material; an in-plane shear stress. In other words, the shear stress causes the crack length to grow along the surface plane. These kind of cracks do not propagate much into the surface and thus tend to be shallow. *Case B* cracks on the other hand, are the consequence of an out-of-plane shear stress and grow into the surface.

Crack growth is influenced by the conditions ahead of the crack tip as well as the stresses behind the crack tip, for which *crack closure* plays an important role. The *stress intensity factor* is used to describe the stress state near the crack tip. Furthermore, it is good to keep in mind that the behaviour of small cracks is different from the behaviour of larger cracks. This becomes clear when assessing the crack growth rate, as small cracks tend to grow faster (until they turn into large cracks; they reach the *long crack threshold*). A well known formula, used to describe (Stage II) crack growth, is the Paris' Law [Paris, 1961], usually presented as:

$$\frac{da}{dN} = C(\Delta K)^m \quad (4.5)$$

in which a is the crack length, N the number of cycles, ΔK the stress intensity factor, C a constant and m a material constant (for metals m generally has a value between 3 and 5).

4.1.1.2 Loading

4.1.1.2.1 Uniaxial and Multiaxial Stress-Strain States It is necessary to discuss the difference between uniaxial fatigue and multiaxial fatigue, as this

complicates the fatigue calculations. Especially in combination with certain loading types, which will be discussed in subsequent paragraphs, the fatigue life calculation can turn into a tedious and complex task.

Multiaxial stress occur very commonly in a wide range of practical situations, while multiaxial strain is in fact quite hard to avoid [Fatemi,] . Multiaxial stresses can be induced by multiaxial cyclic loading, but also by inhomogeneous or anisotropic material characteristics. Multiaxiality implies that the directions of the principal stresses are no longer constant; they vary in time.

4.1.1.2.2 Amplitude and Proportionality When looking at the applied cyclic loads, the behaviour of the amplitude needs to be specified. Basically, the amplitude can either be constant or variable. This seems trivial, but has great consequences. The fatigue damage is computed for each stress reversal or each *stress cycle*. For constant amplitude cyclic loading, the determination of the number of reversals is indeed quite straightforward. Every peak-valley combination counts for one reversal, as the magnitude of the stress for peak and valley are identical. However, when the magnitude is not constant, this obviously poses a problem for the definition of the number of load cycles. Luckily, there are solutions to overcome this problem, the so-called *cycle counting methods*, which will be discussed in more detail in Section 4.1.2.

Apart from the variable amplitude, there is another problem associated with multiaxial fatigue, known as *(non-)proportionality*. The load cycles mentioned before are determined by the maxima and minima of the load history. For (in-phase) proportional loading, the maximum amplitudes of the normal stress/strain and the shear stress/strain coincide. However, for multiaxial stress-strain states this is not necessarily the case, in which case the load is called *non-proportional*. In other words, again, the principal stress directions are not constant. As one could imagine, this poses yet another problem for the determination of the load cycles. The possible solutions for this problem will also be discussed in Section 4.1.2.

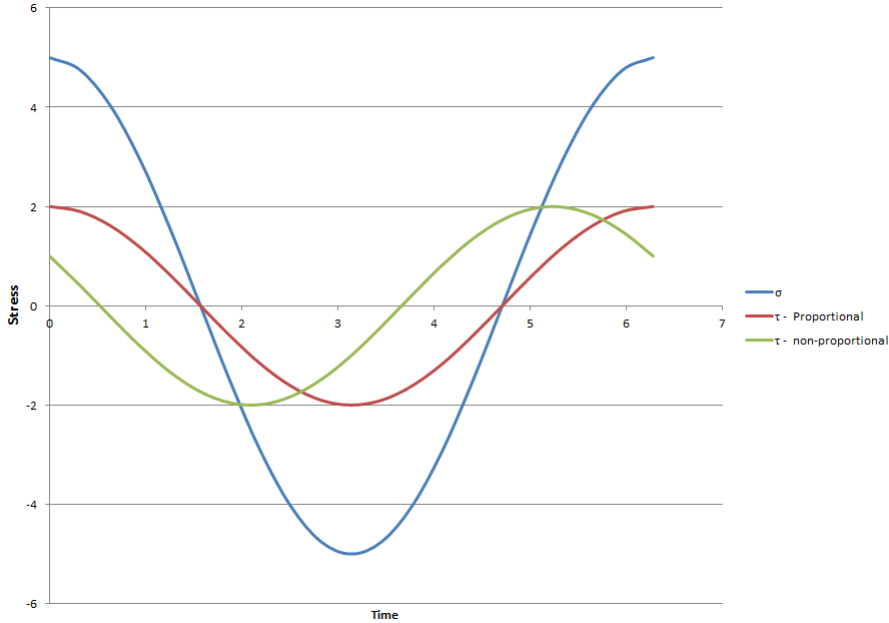


Figure 4.1: Non-proportional loading in the time domain. Its effect is more clearly visualized on a stress-strain plot, see Figure 4.3. (The plot presented here is merely for illustrational purposes, values do not represent real situations)

4.1.1.2.3 Mean Stress In all of the foregoing, one effect has been left unmentioned. When applying a cyclic load, there must be some *mean* load. For ideal cases, for instance a neat sinusoidal uniaxial load, the induced mean stress might be zero and thus have no effect on the fatigue life (the stress state itself may also be called *completely reversed*). However, for variable amplitude and/or non-proportional loading, the mean stress might be non-zero and might not even be constant. It does not take much insight to realize that a mean tensile normal stress will have a negative effect on the fatigue life; simply put, it opens the crack. A mean compressive normal stress might have a positive effect on fatigue life as it basically results in crack closure. As mentioned in [The mean stress effect on the high-cycle fatigue strength from a multiaxial fatigue point of view] a non-zero mean shear stress has no influence on the fatigue life, provided that the shear stress that is applied is lower than the shear yield stress of the material. Both [Susmel et al., 2005], [Ince and Glinka, 2011] give an overview of some commonly applied mean stress corrections, for either multiaxial or uniaxial loading. According to [Socie and Marquis, 2000], for multiaxial stress-strain states, there are basically three approaches to including mean stress effects. The first of these is the modification of the materials' fatigue resistance. This is based on the so-called Morrow mean stress correction. In this method, originally for uniaxial stress-strain states, the mean stress is subtracted from the fatigue strength coefficient. Without going into full details of specific formulations just yet, this approach is illustrated in Equation 4.6,

$$\frac{\sigma'_f}{E} \rightarrow \frac{\sigma'_f - \sigma_{n,mean}}{E} \quad (4.6)$$

in which σ'_f is the fatigue strength coefficient, which is a material property. This type of mean stress correction factors makes no distinction between different crack modes; the effect is assumed the same for both Mode I and Mode II cracks.

The second option to account for mean stress effect is the one used by the so-called Fatemi-Socie model (which will follow in due course). The maximum normal stress during a cycle is used to modify the damage parameter.

The last approach discussed here is the well-known Smith-Watson-Topper model, which only considers Mode I growth. This model is based on increasing the maximum stress by a mean stress. Adopting the same formulation as [Susmel et al., 2005],

$$\sigma_{ar} = \sqrt{\sigma_{max}\sigma_a} = \sigma_{max}\sqrt{\frac{1-R}{2}} = \sigma_a\sqrt{\frac{2}{1-R}} \quad (4.7)$$

In Equation 4.7, σ_{ar} is the equivalent fully reversed stress amplitude. σ_a is the stress amplitude, σ_{max} is the maximum stress and R is the stress ratio (being the ratio of the minimum stress and maximum stress in one cycle, e.g. $R = -1$ for a fully reversed cycle).

In essence, most models that include mean stress into the damage parameters do so by adopting one of the above approaches, in one form or the other. Please note that including mean stress is not limited to stress-based models, but is also applicable to strain-life or energy-based models (all of which will be discussed in due course).

4.1.2 Cycle counting

As was already introduced in the sections on proportionality and variable amplitude (4.1.1.2.2), a fundamental concept necessary to deal with cyclic stresses is the so-called *cycle counting*. Cycle counting enables one to transform a set of variable amplitude loadings into a set of fully-reversed load cycles, which, in combination with some damage criterion, enables the usage of a damage accumulation rule such as Miner's Rule (4.1).

As mentioned before, for a constant amplitude cyclic stress history, cycle counting is unnecessary, as it is easy to define all the reversals. As all peaks and valleys have the same magnitude, every peak-valley combination is fully-reversed. The trouble starts when the stress amplitude is not constant. For such a stress history, the determination of *fully-reversed* cycles is not so easy. This is where cycle counting methods come into play. For fatigue purposes, the so-called *rainflow-counting method* is by far the most popular one, hence this will be the only one presented here. This method will first be introduced briefly here, after which the problems arising for multiaxial non-proportional loading will be discussed.

Consider the time history of the stress or strain as being a sequence of peaks and valleys. Furthermore, the time axis is pointing downwards. Now, imagine the peaks being a series of pagoda roofs. The method is called rainflow counting, because it is now imagined that a rainflow is initiated at the inside of each peak. The rainflow is allowed to drip down, but there are some rules associated

with this. So, the rainflow is allowed to drip down and continue, unless it comes across a more negative minimum than the one it originated from, or a larger maximum than the maximum it initiated at. Rainflows must also stop when they come across a previously initiated rainflow. Also, somewhat intuitive, a rainflow stops when it reaches the end of the time history. With the specifics being in place, the counting can commence. One should count all the rainflow terminations and determine the magnitude of the flow between its starting point and termination point. The stress obtained is for a *half-cycle*. The steps described above should also be performed for the compressive peaks. When this has been done, the half-cycles are matched based on equal magnitude. Two half cycles of equal magnitude but opposite direction are counted as one full cycle [Matsuishi and Endo, 1968] , [Rychlik, 1987] , [Socie, 1982].

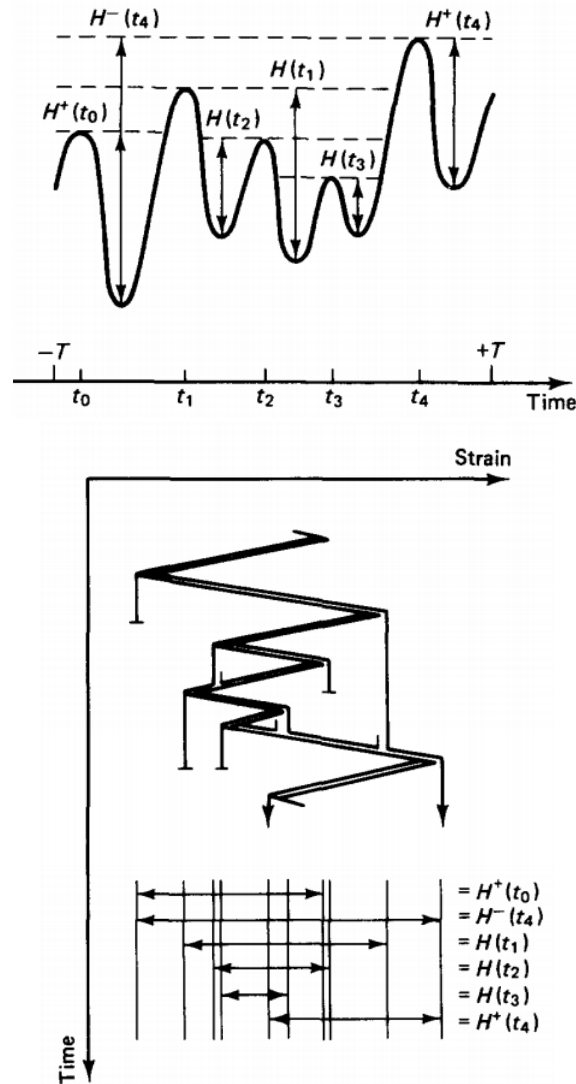


Figure 4.2: Illustration of rainflow counting method (bottom) applied to the cyclic strain-history (top) [Rychlik]

4.1.2.1 Multiaxial rainflow counting

The rainflow-counting above works quite well for uniaxial loading, but for multi-axial loading some problems arise. To illustrate this, a small detour to so-called *hysteresis loops* might be helpful.

There are several different cycle counting methods, the most popular ones being the *Bannantine & Socie* method [Bannantine and Socie, 1991] and the *Wang and Brown* method [Brown and Wang, 1996]. Methods such as the SSF virtual cycle counting method [Anes et al., 2014] are omitted from this discussion as they require quite a few coefficients to be determined by means of experiments and might not have been validated enough. Therefore in this chapter only three

methods will be discussed, the two aforementioned, plus the *modified Wang & Brown* method [Meggiolaro and de Castro, 2012b].

4.1.2.2 Bannantine & Socie

The main idea behind the method proposed by Bannantine & Socie is the *preference* of the material for the type of crack. According to [Socie and Marquis, 2000], either tensile or shear cracks develop within the material. Whether the former or the latter is more damaging, is dependent on the specific material and the stress-strain state. Bannantine & Socie therefore state that both possibilities need to be considered. That means that two damage assessments need to be done; one for the normal strain and one for the shear strain. The steps in this assessment are as follows. First the normal strains are cycle counted, using the uniaxial rainflow counting method. This is allowed as the strains are considered on just one plane in the material; a plane stress-strain state. This is a so-called *critical plane approach* which will be discussed in section 4.1.3.1 in more detail. After all normal strain cycles are counted, some strain-based damage criterion is used to assess the damage. The same steps will then be performed for the shear strain cycles. The strain resulting in the maximum damage will be used for the lifetime calculations. Please note that, in accordance with section 4.1.3.1, all potential planes need to be assessed. As [Socie and Marquis, 2000] states that an increment of 20° will only result in a 20 % error in fatigue life, an increment of e.g. 1° should be sufficient. The Bannantine & Socie method does not take any sequential effects into account and on top of that, it does not take any non-proportionality effects into account. When counting normal stress and shear stress separately, the fact that the respective maxima might not happen at the same time instant is lost.

4.1.2.3 Wang & Brown

If one would plot the axial and shear strain on the vertical axis and the time on the horizontal axis, as is done in Figure 4.4, it is immediately clear why normal rainflow counting will not work. As the axial and shear strain maxima do not coincide, some method to take this non-proportional multiaxiality into account is necessary. For that purpose the earlier mentioned *hysteresis loops* are introduced first.

4.1.2.3.1 Hysteresis loops A hysteresis loop is basically a stress-strain curve, with stress on the vertical axis and strain on the horizontal axis. For an ideal material, in this context meaning perfectly elastic, the stress-strain curve is perfectly linear, with stress and strain being in-phase with each other. One could think of hysteresis as being some sort of inner friction in a material, which introduces some inelasticity. The consequence of the presence of inelasticity, is that for a cyclic stress, the strain is shifted out-of-phase. When translating this to a stress-strain plot, the process is no longer a straight line, but a loop is formed. This loop is called the hysteresis loop. The introduction of [Frunza and Diaconescu, 2006] provides a short, but clear explanation of the concept. More information and illustrations can also be found in [Socie and Marquis, 2000].

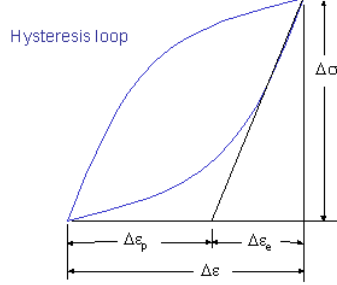


Figure 4.3: Hysteresis Loop [Source: eFatigue.com]

4.1.2.3.2 WB method So, also from the hysteresis loops it is clear that for certain material planes, the maximum stress and the maximum strain do not coincide. This is what causes the problem for most rainflow counting methods.

The most successful multiaxial non-proportional cycle counting method is the method proposed by Wang & Brown ([Meggiolaro and de Castro, 2012b]). Their method is based on the equivalent strain, which is a measure of cyclic plastic deformation. This is closely related to the hysteresis loops and strain hardening [Frunza and Diaconescu, 2006], [Socie and Marquis, 2000].

The equivalent Von Mises stress is introduced because the original Von Mises stress is always positive. The consequence of this is that for a loading 90° out-of-phase, this will result in a constant Von Mises stress, which will lead to an infinite fatigue life ([Meggiolaro and de Castro, 2012b]), as the sign (or direction) of the stress is lost. This is obviously incorrect, so something needs to be done about this.

The Wang & Brown method is based on the relative Von Mises equivalent strain,

$$\varepsilon_{RMises,eq} = \frac{\sqrt{(\Delta\varepsilon_x - \Delta\varepsilon_y)^2 + (\Delta\varepsilon_x - \Delta\varepsilon_z)^2 + (\Delta\varepsilon_y - \Delta\varepsilon_z)^2 + \frac{3}{2}(\Delta\gamma_{xy}^2 + \Delta\gamma_{xz}^2 + \Delta\gamma_{yz}^2)}}{\sqrt{2(1 + \bar{\nu})}} \quad (4.8)$$

in which $\bar{\nu}$ is the effective Poisson's ratio, which is based on the ratio of plastic and elastic strain. Furthermore, $\Delta\varepsilon_x \equiv \varepsilon_{xj} - \varepsilon_{xi}$, $\Delta\varepsilon_y \equiv \varepsilon_{yj} - \varepsilon_{yi}$, $\Delta\varepsilon_z \equiv \varepsilon_{zj} - \varepsilon_{zi}$ and $\Delta\gamma_{xy} \equiv \gamma_{xyj} - \gamma_{xyi}$, $\Delta\gamma_{xz} \equiv \gamma_{xzj} - \gamma_{xzi}$, $\Delta\gamma_{yz} \equiv \gamma_{yzj} - \gamma_{yzi}$, for $j \geq i$. The Wang & Brown method is strain-path dependent, which means that the loading sequence is taken into account [McKeighan and Ranganathan, 2005].

The main rules of the counting method are not different from the uniaxial rainflow counting; the first count must start with the largest ε_{eq} from the complete time-history. The initiation of each count should take place at each peak or valley and should be performed sequentially. The relative strain should be computed with respect to the initial point. Finally, the last point of each count is obtained when reaching: the largest value of ε_{RMises} with respect to the initial point of the history, or coming across a previous path. Please keep in mind that the maxima or minima in each cycle might not occur at the beginning or

end of the half-cycle. This is why the whole path between two reversals needs to be considered.

Instead of identifying the loadcycle directly from the time-history, the relevant path is obtained from the $\varepsilon - \gamma$ plot. In such a plot it is easier to see, where the combination of axial and shear strain is maximized. This point with maximum equivalent strain will be the first point of the first count. Now, the relative equivalent strain is computed, by means of $\varepsilon_{ij}^r = \varepsilon_{ij} - \varepsilon_{ij}^{max}$, which simply relates the relative strain to the maximum strain of the initial point. This step is necessary, because the Von Mises stress is always positive, which would result in the loss of the actual sign of the load. This was explained above. Now, the flow starts, until a maximum with respect to the relative strain of the initial point is reached. The stress range can then be obtained. The method is illustrated in Figures 4.4 and 4.5. In Figure 4.5 only the first loading event is described. The next step would be the count starting at point B, etc. Furthermore, it is necessary to determine the location of auxiliary points like B' in order to not double count any events.

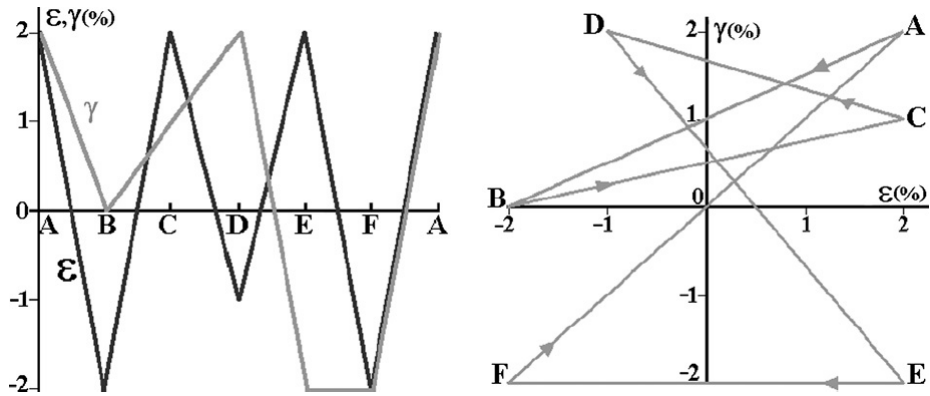


Figure 4.4: Strain history (left) and normal-shear strain plot (right) [Meggiolaro and de Castro, 2012b]

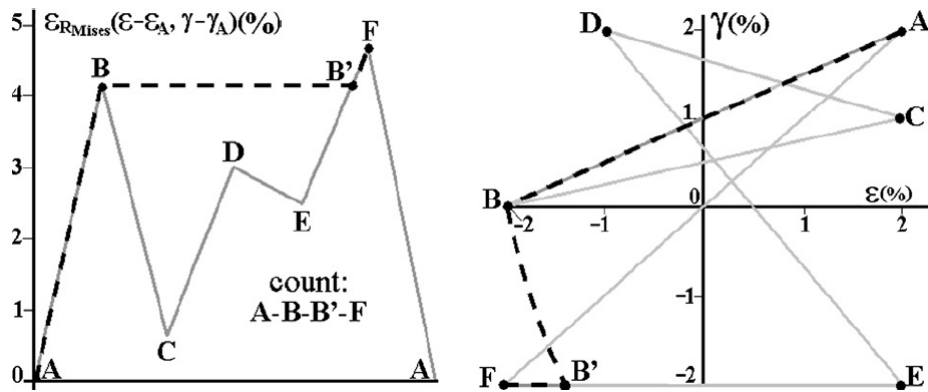


Figure 4.5: The cycle count of the first loading event [Meggiolaro and de Castro, 2012b]

4.1.2.4 Modified Wang & Brown

In their paper [Meggiolaro and de Castro, 2012b], Meggiolaro and Castro have developed a modification to the Wang & Brown method. According to the authors, there are some "idiosyncrasies" associated with the original method. The main modifications are the selection of the starting point of the count and furthermore, the way in which the algorithm is implemented is simplified.

As the authors show, the original Wang & Brown method can sometimes overlook loading events that may be significant for the counting process. For instance, the relative Von Mises strain may reach a peak value, while none of the strain-components has reached a maximum. Their modified version does not overlook these events and thus leads to more conservative fatigue-life predictions. Secondly, they show that the counting algorithm can be simplified by using the so-called 5-dimensional Euclidean space, an approach introduced by [Papadopoulos, 1997]. For plane stress states, this can be reduced further into a 3-dimensional Euclidean space. However, it is deemed too much to go into full details of Euclidean spaces here, the interested reader is referred to [papadopoulos] or their local library. It suffices to say that Euclidean spaces enables one to treat a function of n variables as a point in space. These points in space are treated as a vector, which enables one to use geometrical calculations when studying these functions. Some details of the modified counting method are discussed below, where it should be noted that this is based directly on [Meggiolaro and de Castro, 2012b].

The general multiaxial stress can thus be represented as the set of points $P_i = (S_1, S_2, S_3, S_4, S_5)$, where

$$\begin{aligned}
 S_1 &\equiv \sigma_x - \frac{\sigma_y}{2} - \frac{\sigma_z}{2} = \frac{3}{2}S_x \\
 S_2 &\equiv \frac{\sigma_y - \sigma_z}{2}\sqrt{3} = \frac{S_y - S_z}{2}\sqrt{3} \\
 S_3 &\equiv \tau_{xy}\sqrt{3} \\
 S_4 &\equiv \tau_{xz}\sqrt{3} \\
 S_5 &\equiv \tau_{yz}\sqrt{3}
 \end{aligned} \tag{4.9}$$

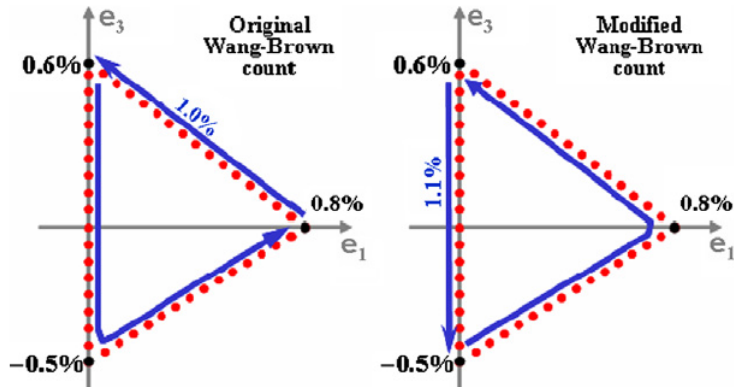


Figure 4.6: The original Wang & Brown method versus the Modified W&B method. As becomes clear from these plots, the modified method takes a more extreme event into account, which was missed by the original method [Meggiolaro and de Castro, 2012b]

Now, the beauty of working in these spaces lies in the fact that the distance between two points is already the relative Von Mises stress between them. At this moment, the actual cycle counting can commence. The first rule of a counting method generally applies to finding the starting point. First select the point that form the longest chord in the 5-dimensional Euclidean stress (or strain) subspace. Among these points one should find the one with the largest distance from the origin. This is point P_1 , the subsequent points remain in their original order. Each count should be initiated sequentially, so the first at P_1 , the second at P_2 , etcetera. As was seen in the opening paragraphs of 4.1.2, some rules need to be formulated for the last point in a count. The termination of a count occurs when a point P_j is reached, which lies farthest away from the starting point. The second termination rule is when a (finite) *segment* from a previous count is encountered. Assuming that the beginning and end of a count have been specified properly, the count itself is formed by the traveled path closest to the straight line between the initial and final points. Please note that this all is still finding place in the Euclidean space.

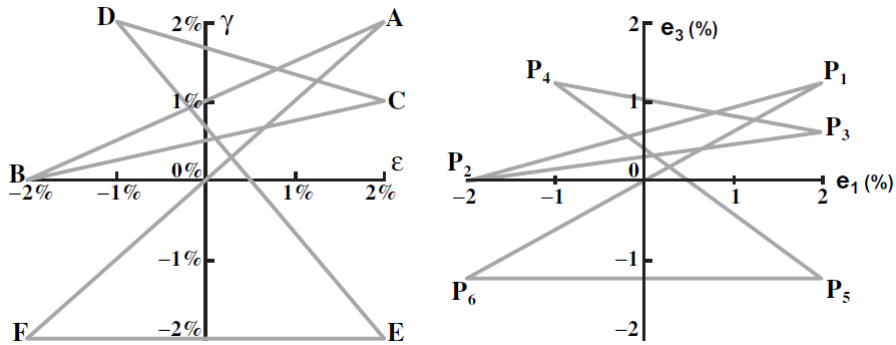


Figure 4.7: The normal-shear strain plot and the 5D Euclidean subspace [Meggiolaro and de Castro, 2012b]

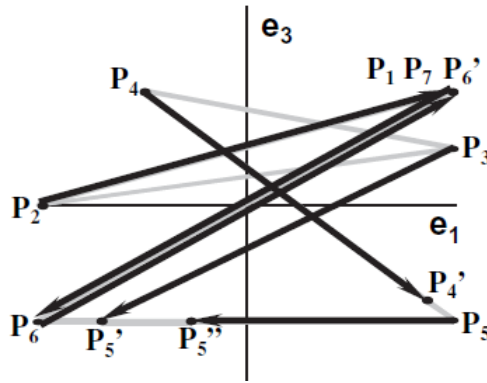


Figure 4.8: The cycle counting method. It is not necessary to recalculate the relative equivalent Von Mises stress for every point, nor is it necessary to work with hyper-ellipses to find the location of auxiliary points [Meggiolaro and de Castro, 2012b]

The equivalent stress (or strain) amplitude of a full cycle (which means two half cycles with identical extreme magnitudes) can be calculated using a convex hull method or the so-called *MoI method* [Meggiolaro and de Castro, 2012a]. A *convex hull method* is basically defining the smallest convex set; the smallest space containing the two points and all the points on a straight line between these points. However, in [paper part I] the authors propose the so-called *Moment of Inertia* method, which is used to obtain the equivalent stress ranges. These two methods are preferable over the original method, as they take the non-proportionality of the path, and the phase difference, into account. The original method makes use of the extreme values, which leads to the loss of the non-proportionality information. What is meant is that the method assumes the methods to occur at the same instant, without taking any sequentiality into account. The MoI method takes the actual loadpath and thus the sequentiality into consideration.

It does so by transforming the 5D Euclidean stress or strain into a 2D loadpath.

The points along the loadpath are then treated as being a 'wire' with unit mass. The mean of the stress can then be assumed to be the centre of gravity of the 'wire'. The center of gravity can be calculated by

$$\begin{aligned} X_c &= \frac{1}{p} \oint X dp \\ Y_c &= \frac{1}{p} \oint Y dp \\ p &= \oint dp \end{aligned} \quad (4.10)$$

The coordinates of the CoG are thus calculated by taking the contour-integrals along the path p . Now the mass moments of inertia can be calculated as:

$$\begin{aligned} I_{XX}^0 &= \frac{1}{p} \oint Y^2 dp \\ I_{YY}^0 &= \frac{1}{p} \oint X^2 dp \\ I_{XY}^0 &= -\frac{1}{p} \oint X \cdot Y dp \end{aligned} \quad (4.11)$$

The subscript ⁰ has been added to point out that this is the mass moment of inertia relative to the origin. These can easily be transformed into mass moments of inertia relative to the loadpath centroid by making use of the parallel axis theorem (Huygens-Steiner Rule):

$$\begin{aligned} I_{XX} &= I_{XX}^0 - Y_C^2 \\ I_{YY} &= I_{YY}^0 - X_C^2 \\ I_{XY} &= I_{XY}^0 + X_C \cdot Y_C \end{aligned} \quad (4.12)$$

The authors then propose the following stress range:

$$\frac{\Delta\sigma_{Mises}}{2} = \sqrt{3 \cdot I_{ZZ}} = \sqrt{3 \cdot (I_{XX} + I_{YY})} \quad (4.13)$$

Finally, the complete fatigue damage can be found. Please note that this is now computed for one plane, for critical plane approaches these steps must be repeated.

When the half cycles are determined, the criteria that will be discussed in Section 4.1.3 can be implemented [Meggiolaro and de Castro, 2012a],[Meggiolaro and de Castro, 2012b].

4.1.3 Criteria

After the occurring damaging loads have been accounted for by means of the cycle counting methods, a fatigue damage criterion is needed to assess the damage and connect it to the number of cycles until failure. A great number of criteria are proposed, however, not all of them are equally successful or accepted. The criteria reviewed in this section are all fairly accepted within the fatigue-community. It should be noted that no criterion is universally accepted for each application. The method proposed by Carpinteri et. al

[Carpinteri and Spagnoli, 2003] in section 4.1.3.1.10 poses somewhat of an exception, as it is slightly more recently proposed.

There are multiple possibilities to assess the fatigue damage, either based on stress, strain or energy. However, not all of these methods are equally suitable for multiaxial loads. The criteria presented here are all based on the so-called critical plane approach. As for multiaxial non-proportional loading the principal stress directions are not constant, it is hard to predict in which direction the crack will grow. In other words, it is hard to predict along which plane the crack will form. Therefore, the critical plane approach aims to take all possible planes into account. The critical plane is deemed the plane on which some damage parameter attains its maximum.

4.1.3.1 Critical plane

This section is dedicated to the so-called critical plane method. The main assumption of this approach is that the fatigue damage gets assessed at different potential material planes. The plane where the damage is greatest, will be the plane where the crack grows along, leading to a means to predict the life.

4.1.3.1.1 Findley Findley used experimental data to arrive at a model that is based on the assumption that the normal stress on a shear plane has a linear effect on the shear stress [Socie and Marquis, 2000]. This is formulated as:

$$\left(\frac{\Delta\tau}{2} + k\sigma_n\right)_{max} = f \quad (4.14)$$

Now, the notion of a so-called critical plane, as mentioned in the introduction to this section, finally comes into play. As the Findley criterion makes use of the stress on a specific plane in the material, this plane must be determined. The general definition of the critical plane is the plane on which some damage parameter takes the maximum value. That means that the way to calculate the orientation of this plane is dependent on that specific parameter, which is the main difference between all critical plane models. According to Findley, the crack growth is dependent on the maximum normal stress and the alternating shear stress. These stresses have to be oriented according to a certain plane, which is done by:

$$\begin{aligned} \sigma_\theta &= \tau_{xy} \sin 2\theta \\ \tau_\theta &= \tau_{xy} \cos 2\theta \end{aligned} \quad (4.15)$$

The correction factor involving k in Equation 4.14 has to be obtained experimentally. [Socie and Marquis, 2000] gives values of 0.2-0.3 for ductile materials. When applying Findley's criterion to finite life fatigue, it assumes the form:

$$\left(\frac{\Delta\tau}{2} + k\sigma_n\right)_{max} = \tau_f^* (N_f)^b \quad (4.16)$$

In Equation 4.16, τ_f^* can be computed from the fatigue strength coefficient, taking into account the k -factor.

Summarizing, the Findley-criterion is based on the maximum combination of the shear stress and the normal stress on a specific material plane. This means that all potential planes need to be considered, for instance at a 1° interval.

4.1.3.1.2 McDiarmid Just as Findley did, McDiarmid [McDiarmid, 1994] analyzed experimental data. After reviewing the high-cycle fatigue data he arrived at a criterion based on the maximum shear stress amplitude. The plane that is deemed the critical plane is the plane on which the maximum shear stress occurs. This can be notably different from the critical plane orientation according to Findley. The damage parameter of McDiarmid is formulated as:

$$\frac{\Delta\tau_{max}}{2t_{A,B}} + \frac{\sigma_{n,max}}{2\sigma_{UTS}} = 1 \quad (4.17)$$

in which $t_{A,B}$ is the shear fatigue strength for either Case A or Case B shear cracking and σ_{UTS} is the ultimate tensile strength. Equation 4.17 can be combined with Basquin's relationship, which leads to an equation for finite life:

$$\frac{\tau_{max}}{2} + \left(\frac{t_{A,B}}{2\sigma_{UTS}}\right)\sigma_{n,max} = \tau'_f(2N_f)^2 \quad (4.18)$$

4.1.3.1.3 Matake The Matake criterion [Socie and Marquis, 2000] is similar to the Findley criterion, generally formulated as

$$\tau_{a,c} + k\sigma_{n,c} \leq \lambda \quad (4.19)$$

However, Matake proposed that the critical plane is the plane where the shear stress attains its maximum, whereas Findley proposed the maximum value of the normal stress (in combination with the shear stress).

4.1.3.1.4 Brown-Miller Brown and Miller formulated a criterion which is based on actual cracking mechanisms. Following the same reasoning as Findley, the shear strain and normal strain are considered the factors contributing to the crack growth. Recalling the crack mechanisms of section 4.1.1.1.2, Brown & Miller propose two separate criteria for each type. For Case A and Case B crack growth, respectively:

$$\begin{aligned} \left(\frac{\Delta\gamma}{g}\right)^j + \left(\frac{\varepsilon_n}{h}\right)^j &= 1 && \text{Case A} \\ \frac{\Delta\gamma}{2} &= \text{constant} && \text{Case B} \end{aligned} \quad (4.20)$$

where g, h and j are constants.

The formulation for Case A cracks was later modified (and simplified) to be:

$$\Delta\tilde{\gamma} = (\Delta\gamma_{max}^\alpha + S\Delta\varepsilon_n^\alpha)^{\frac{1}{\alpha}} \quad (4.21)$$

assuming $\alpha = 1$,

$$\frac{\Delta\tilde{\gamma}}{2} = \frac{\Delta\gamma_{max}}{2} + S\Delta\varepsilon_n \quad (4.22)$$

where $\tilde{\gamma}$ is the equivalent shear strain and S is a material-dependent parameter.

When including Morrow's mean stress, taking elastic and plastic strains into account and defining two parameters A and B dependent on a material parameter S, Brown-Miller is formulated as:

$$\frac{\Delta\gamma}{2} + S\Delta\varepsilon_n = A\frac{\sigma'_f - 2\sigma_{n,mean}}{E}(2N_f)^b + B\varepsilon'_f(2N_f)^c \quad (4.23)$$

4.1.3.1.5 Fatemi-Socie The Fatemi-Socie approach has Brown and Miller's method as a foundation [Fatemi and Socie, 1988]. However, it is based on the normal stress, instead of the normal strain. Furthermore, it aims to take the crack closure effects into account. It does so, by modifying the shear strain with the normal stress. Keeping Brown-Miller (Equation 4.23) in mind, Fatemi-Socie is:

$$\frac{\Delta\gamma}{2} \left(1 + k \frac{\sigma_{n,max}}{\sigma_y}\right) = \frac{\tau'_f}{G} (2N_f)^{b\gamma} + \gamma'_f (2N_f)^{c\gamma} \quad (4.24)$$

Basically, $\frac{k}{\sigma_y}$ is a measure of the influence of normal stress on a material. However, if test data is not abundantly available, $k = 1$ and σ_y is assumed to be equal to σ'_f . The advantage of this criterion is that it not only takes the multiple stress states into account, but can also include mean stress and non-proportional loading.

4.1.3.1.6 Smith-Watson-Topper The Smith-Watson-Topper-criterion (from hereon referred to as SWT-criterion) is developed to model materials that predominantly fail due to tensile stress or strain ([Smith et al., 1970]). These are the cracks that grow on a plane perpendicular to the maximum principal stress or strain. The model was initially meant to model the mean stress effects in uniaxial loading, but also works in analysing non-proportional loaded metals. The formulation of the method takes the principal strain range, $\Delta\varepsilon_1$, and the maximum stress on the principal strain plane, $\sigma_{n,max}$ into account:

$$\sigma_{n,max} \frac{\Delta\varepsilon_1}{2} = \frac{\sigma_f'^2}{E} (2N_f)^{2b} + \sigma_f' \varepsilon_f' (2N_f)^{b+c} \quad (4.25)$$

4.1.3.1.7 Dang Van The Dang Van criterion is based on the concept of microstress within a critical volume of the material [Socie and Marquis, 2000]. The method acknowledges the fact that fatigue crack nucleation is in fact a local process. It has been observed that cracks originate from material grains that have undergone plastic deformation and form slip bands. This was briefly explained in 4.1.1.1.2. As cracks usually start in intergranular slip bands, Dang Van assumes that the (microscopic) shear stress must be important. Following the same reasoning, Dang Van states that the (microscopic) hydrostatic stress will have an effect on the opening of the cracks. This leads to the Dang Van formulation,

$$\tau(t) + a\sigma_h(t) = b \quad (4.26)$$

with $\tau(t)$ and $\sigma(t)$ the instantaneous microscopic stresses. As materials, on the microscopic scale, can no longer be considered homogeneous or isotropic, the stresses will be different from the ones on the macroscopic scale. Grains experiencing the most severe plastic deformation are limited due to the elastic behaviour of adjacent grains. This means that, if no crack will occur, the stresses (and/or strains) need to stabilize. This process is called *elastic shakedown*, which prevents crack growth to adjacent grains. Elastic shakedown is essentially the situation where plastic behaviour occurs during the start up phase (or running in phase), while during the steady state the behaviour is elastic. This can be obtained by strain hardening and/or residual stresses.

It must be noted that Dang Van is an endurance limit. For a loadpath it gives either failure or infinite life.

4.1.3.1.8 Effective Equivalent Stress Hypothesis According to [Sonsino, 1997], the proper way to take the non-proportionality into account for ductile materials is by means of the so-called *effective equivalent stress hypothesis*. The stresses acting on various planes are formulated as:

$$\begin{aligned}\sigma_n(\phi) &= \sigma_x \cos^2 \phi + \sigma_y \sin^2 \phi + 2\tau_{xy} \cos \phi \sin \phi \\ \tau_n(\phi) &= \tau_{xy}(\cos^2 \phi - \sin^2 \phi) - (\sigma_x - \sigma_y) \cos \phi \sin \phi\end{aligned}\quad (4.27)$$

Equation 4.27 follows from considering a surface element and calculating the stresses according to the variable orientation, ϕ , of the surface plane. The EESH assumes that the failure of ductile materials is caused by shear stresses, τ_n in Equation 4.27. The interaction of the shear stresses on various planes is taken into account by creating an effective shear stress, by means of the integral value over all the plane orientations:

$$\tau_{eff} = \frac{1}{\pi} \int_0^\pi \tau_n(\phi) d\phi \quad (4.28)$$

The stress of 4.28 can now be used to calculate the equivalent stress as:

$$\sigma_{eq}(\delta) = \sigma_{eq}(\delta = 0^\circ) \frac{\tau_{eff}(\delta)}{\tau_{eff}(\delta = 0^\circ)} \times \sqrt{Ge^{[1 - \frac{\delta - 90^\circ}{90^\circ}]}} \quad (4.29)$$

with:

$$\begin{aligned}\sigma_{eq}(\delta = 0^\circ) &= \sqrt{\sigma_x^2 + \sigma_y^2 - \sigma_x \sigma_y + f_G^2 3\tau_{xy}} \\ f_G &= \frac{\sqrt{\sigma_x^2 + \sigma_y^2 - \sigma_x \sigma_y}}{\sqrt{3}\tau_{xy}} \\ G &= \frac{1 + \kappa_a^*}{1 + \kappa_t^*} \text{ or } \frac{1 + \kappa_b^*}{1 + \kappa_t^*}\end{aligned}\quad (4.30)$$

In Equation 4.30, G is the ratio of the stress concentration factors κ^* , which can be obtained from Finite Element Analyses.

4.1.3.1.9 Liu & Mahadevan In their paper [Liu and Mahadevan, 2007], Liu & Mahadevan propose the following non-linear damage parameter:

$$\sqrt{\left(\frac{\sigma_{a,c}}{f_{-1}}\right)^2 + \left(\frac{\tau_{a,c}}{t_{-1}}\right)^2 + k\left(\frac{\sigma_{a,c}^H}{f_{-1}}\right)^2} = \beta \quad (4.31)$$

In 4.31, $\sigma_{a,c}$ is the normal stress amplitude, $\tau_{a,c}$ is the shear stress amplitude and $\sigma_{a,c}^H$ is called the *hydrostatic stress amplitude*. These are all acting on the critical plane (hence the subscript c). Furthermore, k and β are material parameters, obtained from uniaxial fatigue limits. The factor k is basically a parameter used to account for the fact that the hydrostatic stress amplitude varies for different materials.

In their model, the authors propose to search for the critical plane as the plane

on which the hydrostatic stress amplitude is zero. To do so, the plane on which the normal stress amplitude is maximal is assumed to be the fracture plane. Subsequently, the angle α between the critical plane and the (assumed) fracture plane is calculated from uniaxial and torsional fatigue test data. When the hydrostatic stress amplitude is equal to zero, equation 4.31 turns into

$$\sqrt{\left(\frac{\sigma_{a,c}}{f_{-1}}\right)^2 + \left(\frac{\tau_{a,c}}{t_{-1}}\right)^2} = \beta \quad (4.32)$$

Now, a fully reversed uniaxial experiment and a fully reversed torsional fatigue experiment will be considered. For the uniaxial data, $\sigma_a = f_{-1}$ and $\tau_a = 0$. The fracture plane is perpendicular to the normal stress direction. The critical plane is oriented with an angle α relative to the fatigue fracture plane. That results in:

$$\begin{cases} \sigma_{a,\alpha} = \frac{f_{-1}}{2} \pm \frac{f_{-1}}{2} \cos 2\alpha \\ \tau_{a,\alpha} = \pm \frac{f_{-1}}{2} \sin 2\alpha \end{cases} \quad (4.33)$$

For the fully reversed torsional case, the critical plane is at an angle α off the maximum normal stress plane. This results in:

$$\begin{cases} \sigma_{a,\alpha} = \pm t_{-1} \cos 2\alpha \\ \tau_{a,\alpha} = \pm t_{-1} \sin 2\alpha \end{cases} \quad (4.34)$$

These results can be substituted into Equation 4.32. This will result in two equations containing α, β and $\frac{t_{-1}}{f_{-1}}$. Defining s as $s = \left(\frac{t_{-1}}{f_{-1}}\right)$, in accordance with [Liu and Mahadevan, 2007], the resulting equations for α and β are

$$\begin{cases} \cos 2\alpha = \frac{-2 + \sqrt{4 - 4\left(\frac{1}{s^2}\right)\left(5 - \frac{1}{s^2} - 4s^2\right)}}{2\left(5 - \frac{1}{s^2} - 4s^2\right)} \\ \beta = \sqrt{\cos^2(2\alpha)s^2 + \sin^2(2\alpha)} \end{cases} \quad (4.35)$$

Equation 4.35 can look somewhat intimidating, but basically it states that, according to Liu & Mahadevan, both α and β are dependent on the material property s . If $s > 1$, it is considered a very brittle material, while $s \leq 1$ describes a more ductile material (to a greater or lesser extent). In turn this means that the critical plane in the present model is not only dependent on the stress state (ie. the maximum normal stress plane), but also on material properties (ie. α). To make the model more complete, Liu & Mahadevan also included the mean stress effect. The mean shear stress effect has been found to have an insignificant influence on the fatigue limit [literature; sines etc] and is therefore neglected. The mean normal stress can then be included by means of a correction factor on the normal stress in Equation 4.31. This part of Equation 4.31 is rewritten as

$$\left(\frac{\sigma_{a,c}}{f_{-1}}\right)^2 \rightarrow \left(\frac{\sigma_{a,c}\left(1 + \eta \frac{\sigma_{m,c}}{f_{-1}}\right)}{f_{-1}}\right)^2 \quad (4.36)$$

The factor η is a material parameter,

$$\begin{cases} \eta = \frac{3}{4} + \frac{1}{4} \left(\frac{\sqrt{3} - \frac{f-1}{t-1}}{\sqrt{3}-1} \right) & \left(\frac{t-1}{f-1} \leq 1 \right) \\ \eta = 1 & \left(\frac{t-1}{f-1} > 1 \right) \end{cases} \quad (4.37)$$

4.1.3.1.10 C-S criterion The C-S criterion was proposed by Carpinteri and Spagnoli in [Carpinteri and Spagnoli, 2003]. Their method essentially consists of three main calculation-steps. In the first step the mean direction of the maximum principal stress is calculated. The so-called *weighted* directions are used for this step. Subsequently, in the second step, an empirical formula is used to couple this direction to the orientation of the critical plane. The last step involves the determination of the fatigue life.

According to the authors, principal stresses are fundamental for the determination of the fatigue life. As the principal stress directions are varying in time, averaged stress directions are used for the life determination. These averaged principal stresses will be computed with the help of weight functions, which, the authors claim, take into account the most important factors influencing the fatigue damage. Euler angles are used to express the principal stress directions, as follows: firstly, the principal stresses are defined as $\sigma_1(t) \geq \sigma_2(t) \geq \sigma_3(t)$. The principal directions are thus labeled 1,2 and 3, respectively. These directions can be described with the Euler angles ϕ , θ and ψ . These angles are essentially three rotations, to describe the orientation of the principal axis system relative to the fixed reference frame. The directions are now specified, but since they vary in time, there is a need to average these directions. In accordance with [Carpinteri and Spagnoli, 2003], the averaged directions and averaged Euler angles are labeled $\hat{1}, \hat{2}, \hat{3}$ and $\hat{\phi}, \hat{\theta}, \hat{\psi}$, respectively. The averaged Euler angles are calculated as:

$$\begin{aligned} \hat{\phi} &= \frac{1}{W} \int_0^T \phi(t) W(t) dt \\ \hat{\theta} &= \frac{1}{W} \int_0^T \theta(t) W(t) dt \\ \hat{\psi} &= \frac{1}{W} \int_0^T \psi(t) W(t) dt \\ &\text{with } W = \int_0^T W(t) dt \end{aligned} \quad (4.38)$$

In Equation 4.38, $W(t)$ is the weight function. T is the observation time. The weight function is formulated as

$$W(t) = h \left[\sigma_1(t) - \frac{1}{2} \sigma_{af,-1} \right] \left(\frac{\sigma_1(t)}{\sigma_{af,-1}} \right)^{-\frac{1}{m}} \quad (4.39)$$

where h is the Heaviside function and m is the slope of the S-N curve for fully reversed normal stress. The origin of the factor $\frac{1}{2}$ in the square brackets is not completely clear [Papuga, 2007]. The authors have developed the so-called *C-S*

criterion for different cases and situations. Here, only the general loading case will be discussed.

The scalar value of the normal stress vector, $\vec{N}(t)$ will be the cycle counting variable. The direction of this vector is constant in time, as opposed to the shear stress vector $\vec{C}(t)$. The sequence N_i is now reduced to a sequence that does not consist non-extreme values, which results in the sequence N_j^* . The same instants are removed from the sequence C_i , resulting in the sequence C_j^* . However, this might eliminate maximum shear stress values, as they do not necessarily coincide for non-proportional multiaxial stress states. Therefore, the authors implement a reduction method to obtain C_j^* , that retains the maximum shear stress values. The method is formulated as follows. The time instants corresponding to two consecutive extreme values of N_i are denoted as i and $i + K$. For $k = 1, 2, \dots, K$, the mean value and amplitude for two vectors C_i and C_{i+k} are calculated as $C_m^{(i,i+k)}$ and $C_a^{(i,i+k)}$. The next step is to retain the vector $C_{i+\bar{k}}$ where \bar{k} is the value of k for which $C_a^{(i,i+k)}$ reaches its maximum value. The resulting sequence is C_j^* . When both reduced sequences are computed, the maximum value $N_{max,z}^*$ for the z-th resolved reversal can be obtained by means of the rainflow cycle counting of N_j^* . Furthermore, the amplitude $C_{a,z}^*$ can be obtained from C_j^* . Now, the equivalent stress can be calculated according to

$$\sigma_{eq,a} = \sqrt{\left(N_{max,z}^*\right)^2 + \left(\frac{\sigma_{af,-1}}{\tau_{af,-1}}\right)^2 \left(C_{a,z}^*\right)^2} \quad (4.40)$$

The authors of [Carpinteri and Spagnoli, 2003] call Equation 4.40 equivalent stress, but in essence this is the damage criterion. The author of this thesis has adopted the original papers' terminology.

An empirical formula to determine the angle between the maximum principal stress and the normal to the critical plane is proposed as

$$\delta = \frac{3\pi}{8} \left[1 - \left(\frac{\tau_{af}}{\sigma_{af}} \right)^2 \right] \quad (4.41)$$

Equation 4.41 is used to determine the plane on which the following fatigue assessment should be performed. It is also possible to implement a maximum damage instead of the original proposal's solution for the critical plane.

To compute the cumulative damage, the authors propose to use a non-linear damage rule [Čačko, 1999],

$$D(T_0) = \sum_{z=1}^Z (D_z)^q \quad \text{with } D_z = \begin{cases} \frac{1}{2N_0} \left(\frac{\sigma_{af,-1}}{\sigma_{eq,a,z}} \right)^{\frac{1}{m}} & \sigma_{eq,a,z} \geq 0.5\sigma_{af,-1} \\ 0 & \sigma_{eq,a,z} \leq 0.5\sigma_{af,-1} \end{cases} \quad (4.42)$$

with

$$q = 1 + \frac{0.25}{0.5\sigma_{af,-1}} (\sigma_{eq,a,z} - \sigma_{af,-1}) \quad (4.43)$$

4.1.3.2 Comparison

When looking at the different approaches discussed in the previous sections, one should keep in mind that the multiaxial fatigue problem does not have a well-established theory, that covers all materials, loads and gives a perfect life

prediction. As fatigue experiments are cumbersome to perform, and take up a lot of time and money, there is not much multiaxial data readily available. Usually, validation by means of experiments is done for one or two types of steel and only one geometry. So, as the number of data sets used for validation is usually fairly small, some theories might show good agreement for the used data, but changing the material, loading or geometry might result in less realistic (life) predictions.

For the present work it might be hard to predict which criterion will show the best agreement. As stated previously, the criteria presented here are the more well-established criteria, often recurring in literature on the subject.

4.2 Mooring chain link

This section will elaborate on some of the characteristics of offshore mooring systems, especially the mooring chains. The descriptions of mooring systems is intended as context for the work presented in this study. Furthermore, this chapter will clarify the nature of the problem, with focus on the multiaxiality of the loading.

4.2.1 Mooring systems

In recent times, the quest for fossil fuels has driven oil companies to offshore locations. Crude oil is pumped up from the sub-sea oil-well onto Floating Production, Storage & Offloading vessels (from hereon referred to as FPSO's). The petroleum produced on these FPSO's is transported to the mainland by means of (smaller) oil tankers or pipelines. This chapter will not focus on subsea systems, offloading mechanisms or production. Those subjects are worth a separate study and are therefore beyond the scope of this work. For the present purposes it suffices to see the FPSO as a large *stationary* oil tanker, with production systems on its deck. It must be noted here that the use of mooring systems and/or chains to connect a vessel to the sea-bottom are not limited to FPSO's, but are also used to fix e.g. calm buoys [Jean et al., 2005]. The term vessel in this chapter therefore refers to floating units, intended for the oil & gas industry.

The fact that an offshore vessel operates on the same location for a longer period of time (\sim years) is an important characteristic. As was discussed in previous sections, fatigue is a phenomenon that comes into effect after a (large) number of loading cycles. As the vessel is stationary, the mooring system will experience an extended period of cyclic loading, due to the constantly incoming waves. As the vessel keeps stationary for at least multiple months (but often years), some sort of system is needed to keep it at its place. Dynamic positioning, an automated system keeps the vessel in a specific position by means of thrusters, is not feasible for these applications. It is not hard to imagine that the costs of running the vessels engines or generators continuously for a period of 20 years would be astronomical, not to mention the extra maintenance and other related costs. Therefore, the only feasible station-keeping method is a mooring system that involves anchors and chains.

There are several options to moor a vessel to the seabed, most notably the *turret moored* system and the *spread moored* system.

A spread moored system is a system consisting of multiple clusters of (multiple) mooring lines. These clusters are spread out along the vessel (typically four clusters, one at every 'corner'). This set-up means that the heading of the vessel is fixed. Usually the bow of the vessel is in the direction of the highest waves.

The turret moored system is usually preferable (depending on economic feasibility), because it does not fix the heading of the vessel. This means that the bow is always aimed at the direction from which the worst environmental conditions originate. This behaviour is called *weathervaning*, the way this works will follow. The mooring chains will be connected to the turret at the *chain table*. This part is in turn connect to the vessel by means of a bearing. So, the chain table and the turret/vessel can rotate relative to eachother. As the mooring chains are anchored at the seabed, the chains and chain table stay more or less stationary, while the vessel rotates in the direction of the 'weather'. However,

there will be some friction in turret bearing, which means that some torque must be applied before the bearing rotates. This is called the breakout torque. This effectively results in the chain experiencing an angle with the vessel, in the period before the torque is high enough to make the bearing rotate. This concept is important to keep in mind for the next section.

That is, in short, the turret system. There are multiple configurations possible, such as a cantilever turret, a column turret or an internal turret, each with its advantages and disadvantages. The different systems will not be discussed in-depth here, as it lies outside of the scope of this work.

4.2.2 Out-of-plane bending

Out-of-plane bending (OPB) has only recently been found to be a failure mode of mooring chains. As a consequence, the amount of literature on the subject is fairly limited. Most literature and information leads back to a joint industry project (JIP) led by SBM [Jean et al., 2005]. This JIP investigated the unexpected failure of mooring chains of a buoy that occurred after only half a year of service. The JIP succeeded in recognizing the mechanisms that led to the failure. These mechanisms will be discussed here first, after which some remarks will be made that lead to the justification of the present work.

According to [Jean et al., 2005], several mooring chains of the Girassol Buoy ruptured almost at the same instant, after being about 235 days in operation. Strikingly, the ruptures (or severe cracks) were found to occur in the same chain link for all mooring chains. As the ruptures all occurred in the fifth chain link, it was suspected that some unknown mechanism was causing the failure.

When thinking about chains, one would not expect a chain to have bending stiffness. Indeed, as a chain can be put in practically any shape, it appears to have no stiffness against bending, unlike e.g. a (Timoshenko or Euler-Bernoulli) beam. This is true for chains under low tension, but it appears that a high tension induces a bending stiffness in the chain (this is the reason that OPB is mostly a problem for deepwater mooring). Under high tension the individual chain links can no longer rotate unobstructed between consecutive links. This turned out to be caused by the deformation of the contact area between two links. As the high tension during proofloading (permanently) deforms the contact area, under high operational tension the links tend to 'lock into each other', which is why this mechanism was aptly named *locking mode*. So, the links cannot roll freely anymore, which means that the chain now has a bending stiffness and will behave more like a beam. According to [Jean et al., 2005], the bending stresses generated in the links are large enough to explain the failure of the links. As the waves keep exiting the vessel, bending stresses have a cyclic nature and will cause crack propagation, ultimately accumulating to fatigue failure.

The JIP was very successful in determining the mechanisms involved and trying to produce countermeasures against OPB induced failure. However, the fatigue analysis seemed to be somewhat neglected. In [Jean et al., 2005], the authors make use of an S-N curve given by DNV standards. First of all, an S-N curve does not give the fatigue life, as it assumes infinite life for stress ranges below the selected curve. Second of all, for damage calculations BV suggests the Dang Van criterion, which does not show a good agreement for non-proportional loads [Socie and Marquis, 2000], [BV, 2014]. As the OPB loading has a non-proportional character, the fatigue assessment could possibly be enhanced by

selecting a more appropriate fatigue criterion. The present work aims to find such a criterion and consequently improve the fatigue-life prediction for OPB fatigue failure.

5. Problem statement

5.1 OPB Problem

This chapter briefly repeats the problem statement, with some more focus on practically solving it.

The proofloading of a chain section of a mooring line causes the contact surface of the chain links to deform. As the contact surfaces deform, the chain link movement/rotation relative to each other is restricted. This is called the interlocking of the chains. As the chain links are locked together, the chain starts behaving more like a bending beam. This means that the chain all of a sudden has a bending stiffness. Due to the vessel motions, a bending moment is induced in the chain link. As a consequence of the periodic nature of the loading, fatigue effects come into play.

The motions of the chain are not restricted to one coordinate plane, meaning that the fatigue analysis needs to take this multiaxiality into account. As motions do not necessary occur in-phase, the analysis is further complicated by non-proportionality effects.

5.2 Solution method

The proposed method to analyse the fatigue behaviour of the chain link is discussed next.

To be able to assess the fatigue damage, a damage criterion needs to be implemented. These criteria have been discussed in the literature review (4.1.3). Most criteria are based on combinations of normal and shear stresses or strains. To acquire these stresses along with the loading data, a finite element model needs to be constructed. This model needs to be capable of taking non-linear contact effects into account. The output of the FE model should be the input for all fatigue damage criteria. As the OPB fatigue damage is of interest, only the area where multiaxial stresses occur will be reviewed. These areas can be determined from the results, in accordance with previous OPB research and guidance notes provided by Bureau Veritas.

Once the relevant stresses and/or strains are obtained, the fatigue calculations can commence. The fatigue calculations will comprise a cycle counting method, which can be the Bannantine & Socie approach or the Wang & Brown method. Once the stresses/strains, or rather the ranges, are counted, the next step involves inputting them in the damage criteria. These criteria can then give a Fatigue Index, being a measure of the damaging effects. The damage criteria can also be linked to the (expected) number of cycles to failure. This could eventually lead to a fatigue-life prediction.

5.2.1 Software

5.2.1.1 Ansys

For the Finite Element part of the analysis, Ansys FE software will be used. This software suite is one of the leading packages on the market and used for a wide range of applications in both research and professional environments. It is assumed that this software suite does not need a further introduction. The finite element method will be discussed in a few moments.

5.2.1.2 Pragtic

Pragtic is a freeware software, based on the PhD-dissertation work of ir. J. Papuga, a researcher from the Czech Republic [Papuga, 2005]. The goal of the software is to provide for a simple way to do an automated fatigue calculation. To do so, one loads results of the Finite Element calculation into the Pragtic software after which a range of fatigue methods can be implemented. The software enables one to set up all parameters of the method in detail, which is not always the case with other commercial software. Also, as there is not always a clear description of how the method is implemented, for multiple degrees of freedom, wrong settings can lead to seemingly plausible results. The Pragtic software offers a range of background information and leaves a lot of settings and/or input to the user. This might be slightly more difficult or time-consuming, but hopefully, this will enable users (with some knowledge of the fatigue backgrounds) to obtain more realistic results.

6. FE Analysis

In this chapter the chain link model used in the fatigue analyses will be presented. As this research focuses on the chain link itself, the chainstopper and clacker have been omitted from the used model. In reality, these parts are necessary to review the behaviour of the mooring chain under OPB loading. However, for the present purposes, the multiaxial fatigue analysis of the chain link most susceptible to damage is sufficient. The constraints imposed on the model should make sure the relevant real-life behaviour is preserved.

Modeling is done in accordance to the limited guidance Bureau Veritas gives on the subject. The chain type is in accordance with manufacturer data and is a chain often used by LMC, where this thesis research was conducted.

This chapter starts with some background information on Finite Element Analysis and the relevant details for this model. Next, the model geometry, loads and constraints are presented. The loads and displacements imposed on the model follow mostly from LMC calculations. Some limitations with respect to the analysis that might be present are discussed next. Finally, the solution from the stress analysis will be presented.

6.1 Finite Element Analysis

This section will present an analysis method known as Finite Element Method, which is the preferred method for most engineering calculations. The Finite Element method is used for many different engineering applications, ranging from thermal, structural to fluid engineering. However, in the present discussion, the focus will be on the structural application only.

In engineering, very often problems arise for which one would like to obtain the displacements, deformations or stresses in the material. For some simple situations, this can be done analytical. However, for most real-life situations, the structures and loading can be quite complex, making it hard or impossible to solve analytical. For such applications, Finite Element Analysis can give a numerical approximation of the solution. The main concepts of the method will briefly be discussed next, however, this is not intended as a complete mathematical elaboration of the method.

6.1.1 Finite Elements

For engineering purposes, the main output one desires from calculations are displacements, deformation and stresses. The trouble is that the calculations are based on (multiple) differential equations, some of them partial differential equations. This is what makes it practically impossible to analytically solve complex structures, so a way around this problem is needed. If an analytical solution cannot be found, it might be possible to find an approximation. The FE Method does so by dividing the complex continuous system into many simple systems. The necessary equations are then applied to that simpler (and often: smaller) subdomain, which are called *finite elements*. All these smaller elements are connected to each other at points called nodes or boundary lines or surfaces. By preserving the connection, the results are essentially a boundary condition

for the next element.

For engineering purposes, usually the first unknown is the *displacement*. The algebraic equations can be solved for the nodal points, where an approximation or *shape function* is introduced to find values for the displacement inbetween the nodes. So, essentially, the displacement function is approximated by many small/simple elements, which in turn are substituted into the governing equations. With the help of the boundary conditions (6.1.2) this leads to a linear system of with the number of unknowns equal to the number of equations. This can be solved, which leads to the displacement function. Together with geometry, material properties and other relevant data, these equations eventually allow calculations of stress and strain.

6.1.2 Boundary Conditions

To be able to solve differential equations, the condition at the boundaries of the domain need to be known. A boundary condition can specify the solution of the differential equation at a point in space, but can also specify the solution at a point in time. Likewise, it could also specify the value of a derivative at a certain point in space or time. The specification of imposing both the solution value and the derivative of the solution is called a *Cauchy* boundary condition. In the world of structural engineering, an example of a boundary condition is specifying a zero displacement in a particular direction on one end of a beam. The chain model presented in section 6.2 will clarify boundary conditions more.

6.2 FE Chain link model

This section will present the chain link model used to calculate the stresses and strain that occur in the chain link during OPB loading. The relevant modeling considerations will be clarified accordingly.

6.2.1 Geometry & Material

The chain link used is the so-called Grade R4 chain link. The specification is based on the ABS Rules regarding mooring chains, which are adopted by most class societies. All the relevant data with respect to these chains is summarized in Table 6.1 . For the present calculations, it is assumed that the chain is initially undeformed and uncorroded. The dimensions of the chain link are presented in Figure 6.1, which can be obtained from the manufacturer, Vicinay.

| Property | Symbol | Value |
|---|----------------|----------|
| Young's Modulus | E | 200 GPa |
| Ultimate Limit Strength | σ_{uts} | 860 MPa |
| Yield Strength | σ_y | 550 MPa |
| Friction | μ | 0.16 |
| Fatigue Strength Coefficient | σ'_f | 1700 MPa |
| Fatigue Strength Coefficient in Torsion | τ'_f | 900 MPa |
| Fatigue Strength Exponent | b | -0.139 |
| Fatigue Ductility Exponent | c | -0.498 |
| Cyclic Hardening Coefficient | K' | 2200 |
| Cyclic Hardening Exponent | N' | 0.272 |
| Fatigue Limit in Reversed Tension | σ_{fl} | 430 MPa |
| Fatigue Limit in Reversed Torsion | τ_{fl} | 250 MPa |
| Socie constant | Csoc | 1 |
| Shear Modulus | G | 80 GPa |

Table 6.1: Material properties



DATA SHEET

| QUALITIES | CLASS. SOCIETY | TYPE | STUDLESS |
|-----------|----------------|----------------|-----------------|
| R4 | ABS-R4 | STUDLESS CHAIN | 101 COMMON LINK |

COMMON LINK FOR 124 mm STUDLESS CHAIN
 Material Quality: ABS-R4
 Project: _____

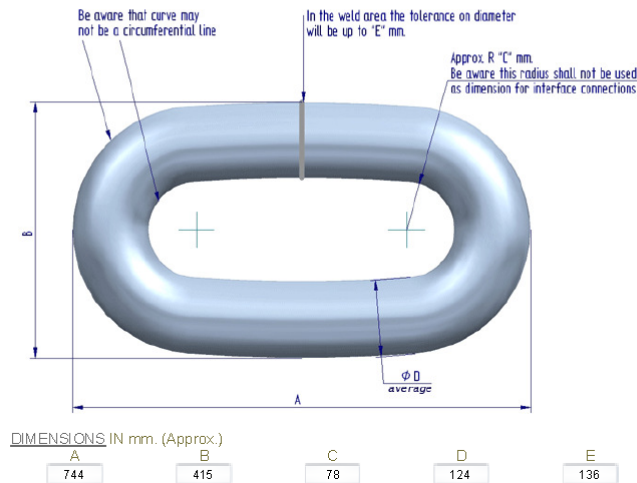


Figure 6.1: Geometry of a common Grade R4 chain link

The chain links are modeled in Ansys FE software, as introduced in 6.1. For the present purposes, it is deemed sufficient to model one complete link, connected to two half links on each side. However, for the present problem, 4.5

links have been modeled, to keep the local effects from the load and translation application relatively far from the investigated link. The stress analysis will be performed on a complete link, which is referred to as the OPB link from hereon. This method is based on the BV Guidance notes on OPB of mooring chains [BV, 2014].

6.2.2 FE: Loads, constraints & mesh

6.2.2.1 Loads & Constraints

To mimic the real-life loading, the loading on the model is applied as follows. To model the proofload, a tension of 11319 kN is applied to the chain link, in accordance with the 80% of the maximum breaking load, used in the industry. This will induce the deformation of the contact area, which will result in the interlocking of links. Subsequently, a motion is applied to the 'lower' link. This effectively simulates the vessel's motion and will induce the alternating load. The angles and associated displacements will be summarised in Table 6.2. The displacement applied to introduce the bending moments in the link will be time-dependent, so that effectively a motion is introduced. In accordance with the aforementioned Guidance Note, one of the half links is fully constrained.

The loading of the chain is done by means of imposing an axial load of 2877 kN, which represents the tension, and moving the chain link. The loaded link is the link on the utmost left end from the studied (middle) link. Before the motion is performed, the chain is proofloaded. This should deform the contact surface, which will result in the aforementioned locking of the chains. After this step, the movement of the chain will be implemented, rotating the adjacent link by different angles in multiple timesteps. To introduce some non-proportionality, two different angles will be implemented, loading the link both in- and out-of-plane. This behaviour relates to the chain being bend by the vessel rotating as well as the vessel translations in both the horizontal plane and the vertical direction. In each time step the problem will be statically solved. All timesteps together will effectively lead to a transient analysis, with changing equilibrium conditions. The choice of this method is governed by subsequent fatigue calculations. During the rotation, the load will be oriented to always be axial, as it represents chain tension.

The imposed angles are presented in Figure 6.2.

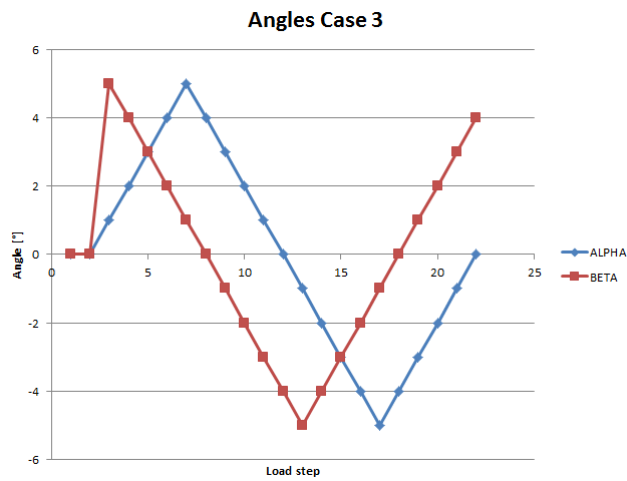
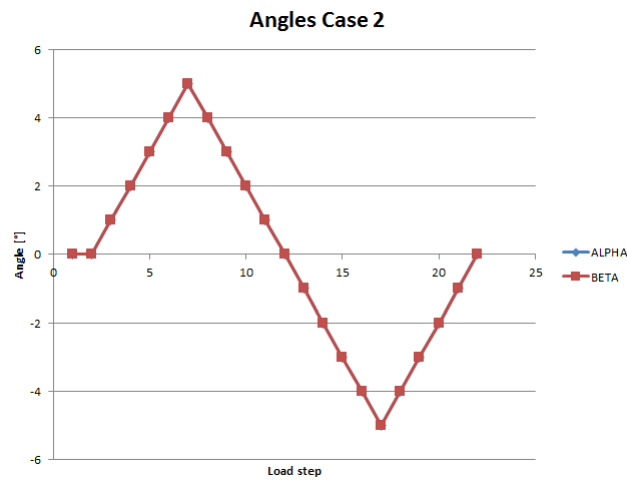
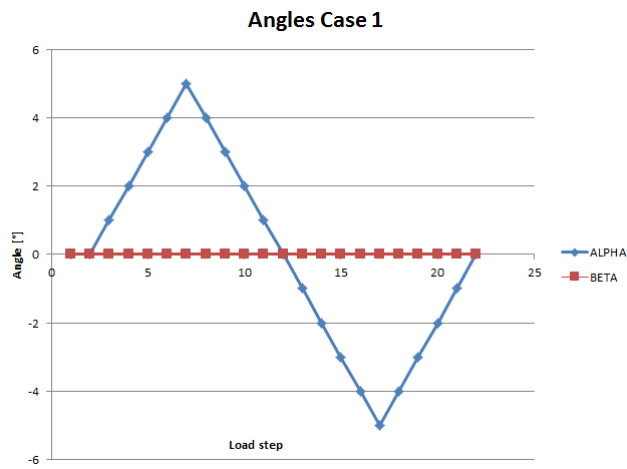


Figure 6.2: Plots of the angles imposed on the lower chain link

In the present calculations, the axial load is applied in two subsequent load-steps, after which the translation of the lower chain link commences. The first simulation will move the link over a range of 10 degrees, so an offset of 5 degrees on each side of the starting condition. This displacement will take place over 20 different timesteps. In subsequent analyses, a phase difference between the two angles can be implemented, as well as different angular ranges. The main cases being examined are presented in Table 6.2. Due to time limitations, more simulations will not be run. However, these three cases should give at least some overview; Case 1 examines purely out-of-plane loads, Case 2 examines the combination of out-of-plane and in-plane loads, while Case 3 examines the effect of a phase difference between the two angles. The phase difference was quite randomly chosen, shifting the maximum value of β to the first non-zero timestep (loadstep 1 and 2 are zero, to put tension on the chain). The phase shift effectively is a shift by 4 seconds. So the angular phase difference then turns out to be $\gamma^\circ = \Delta t[s] \times (360[^\circ] \times f[1/s]) = 72^\circ$.

| Case | α | β | γ |
|------|----------|---------|----------|
| 1 | 10° | 0° | 0° |
| 2 | 10° | 10° | 0° |
| 3 | 10° | 10° | 72° |

Table 6.2: Simulation parameters

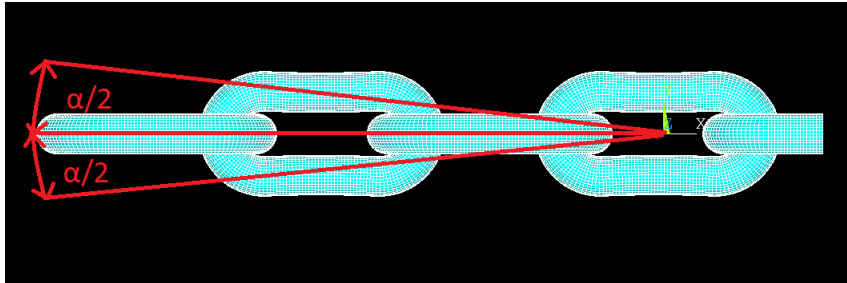


Figure 6.3: The angular range, which will be imposed via a translation of the lower (left) link. The angle in the horizontal direction is similar, but in the horizontal plane. As the third link is the link of interest, alpha imposes a out-of-plane angle, while beta (in the xz-plane) is the in-plane angle.

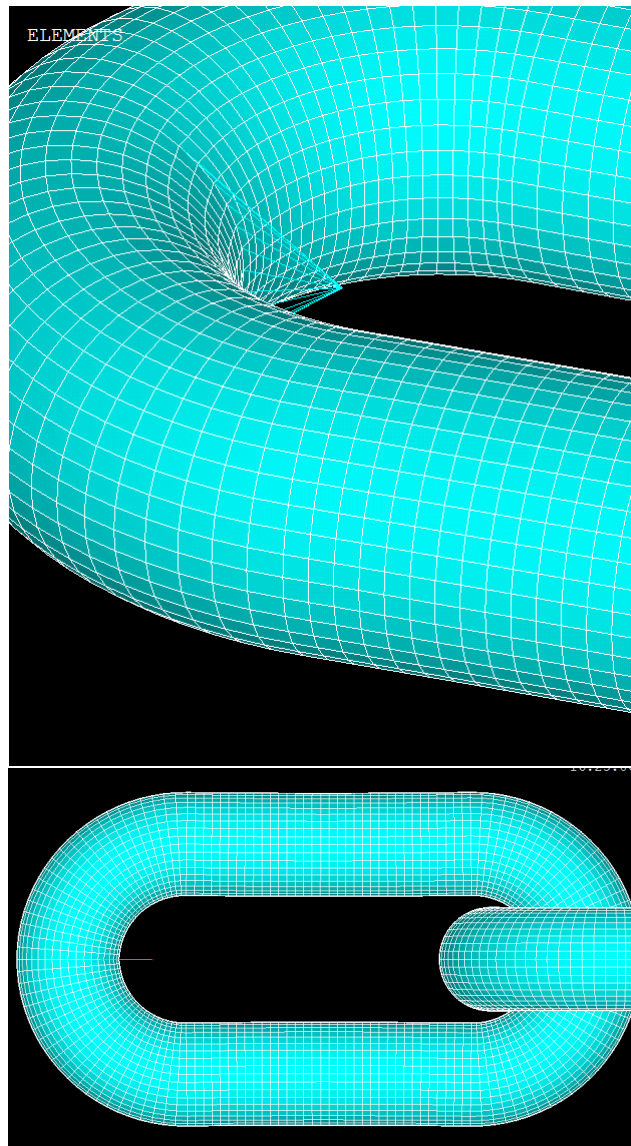


Figure 6.4: The point where the force/translation is applied and transferred to the link. The point where the force and translation is applied corresponds to the center of gravity of the 'next link'. The blue lines are beam elements, while the link itself consists of solid elements.

6.2.2.2 Meshing

As was explained in the chapter on FEA, the model needs to be divided in many small elements. This is done by generating a *mesh*. There are many mesh types available, each with its own properties, advantages and disadvantages. The element types used in the present model are *SOLID185*, *BEAM188*, *CONTA174* and *TARGE170*.

Generally speaking, 3D solid elements, such as SOLID185, are the most precise element types, capable of modeling the behaviour in three degrees-of-freedom at each node. However, this comes at the cost of computational effort and time. For many applications, this degree of detail is not required. For some problems, the behaviour in some degrees of freedom are negligible, which means that a solid element is not necessary to solve the problem adequately. For a large plate with a relatively small thickness, the stress through the thickness might not always be necessary, for instance. The next paragraphs will specify some properties of the used element types and explain why they are used for the present model.

SOLID185 The SOLID185 is a three-dimensional structural solid, defined by 8 nodes per element. Each node has three degrees-of-freedom, namely a translation in X-, Y- and Z-direction. The main advantage for the present application is the fact that it is capable of taking plasticity, stress stiffening, large deflection and large strain effects into account. Since out-of-plane bending is inherently a non-linear problem, the element type should be able to take this behaviour into account. SOLID185 is the most current solid element, with most non-linear options available.

BEAM188 The BEAM188 element type consists of two nodes, each with six degrees-of-freedom, namely translation along the three axes and the rotation around the three axes. The element type is based on the Timoshenko-beam, which takes shear effects into account. For this particular application, the beam elements are not needed with full capacity, as they are only implemented to apply the force and/or displacements to. The sectional properties are such that they do not deflect themselves, but transfer the force and displacement to the solid element. The beam elements can be seen as red lines on the most left link, in Figure 6.5.

CONTA174 The CONTA174 element is used to model the contact and sliding behaviour of the links. The element has 8 nodes, with three degrees-of-freedom; translations in X-, Y- and Z-direction. This contact element is recommended for overlaying most solid elements, including SOLID185 elements. With overlaying is meant that the CONTA174 element is applied to the surface of the solid elements, with whom they share geometric properties. In other words, the CONTA174 elements follows the shape of the underlying solid elements. To completely model the surface-to-surface contact, the CONTA174 elements are associated with their target elements, TARGE170 in his case.

TARGE170 The TARGE170 element, specifies the surface with which the deformable surface (CONTA174) is in contact. The nodes of the target surface have three translational degrees-of-freedom. In the present model, the contact surface of the half links are modeled by TARGE170 elements, while the contact surfaces of the OPB link are modeled with CONTA173 elements. Both CONTA173 and TARGE170 are suitable for nonlinear calculations. This is not completely surprising as most contact processes are inherently nonlinear.

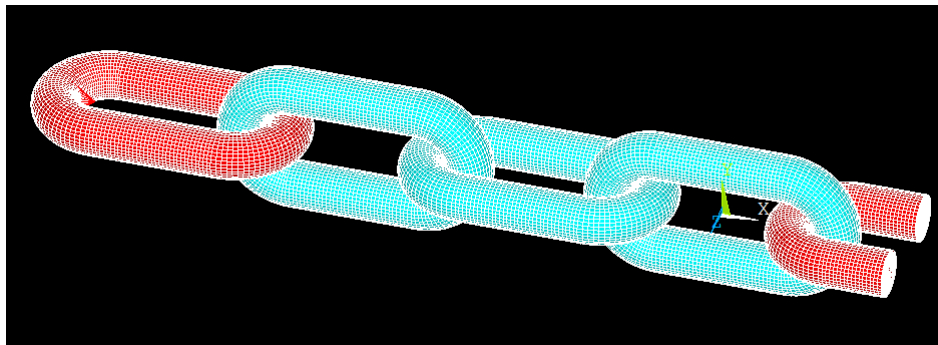


Figure 6.5: Plot of the meshed model. The red links have an elastic formulation, while the middle three blue links have an elasto-plastic formulation

6.2.2.3 Plasticity

To account for the chainlink deformation due to the pre-tension, *plasticity* needs to be included in the Ansys simulation. Even though most readers will be familiar with terms as elasticity and plasticity, for the sake of completeness they will be briefly repeated here.

Elasticity can be described as the tendency of the material to return to its original shape after unloading. If the stresses are below the yield strength, the behaviour is called the elastic response. When looking at the atomic roster of metals, elasticity is the stretching of the bonds between the atoms, but *not* the breaking of the bonds. Elastic behaviour can be adequately described by Hooke's Law, which is a (linear) stress-strain relationship that is formulated as: $\sigma = E\varepsilon$.

Plastic behaviour on the other hand, results in a permanent deformation even though the load is removed. On the atomic level, this means the introduction of slip between planes, which means that the atoms rearrange themselves. The stress-strain curve is schematically presented in Figure 6.6

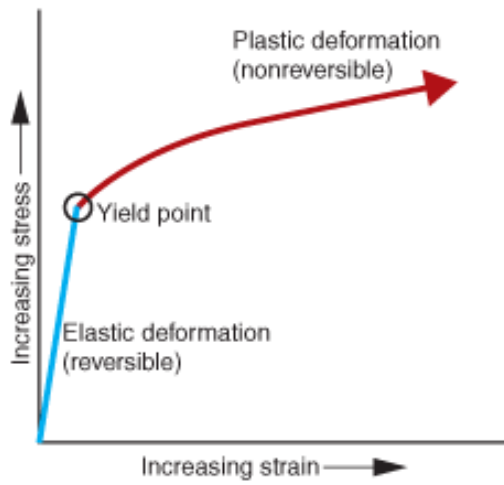


Figure 6.6: Stress-Strain curve. Note the different regions.

The curve implemented in ANSYS is the so-called bilinear kinematic hardening curve, taken from LMC reports [Golisz, 2015], which in turn are based on ASME-definitions.

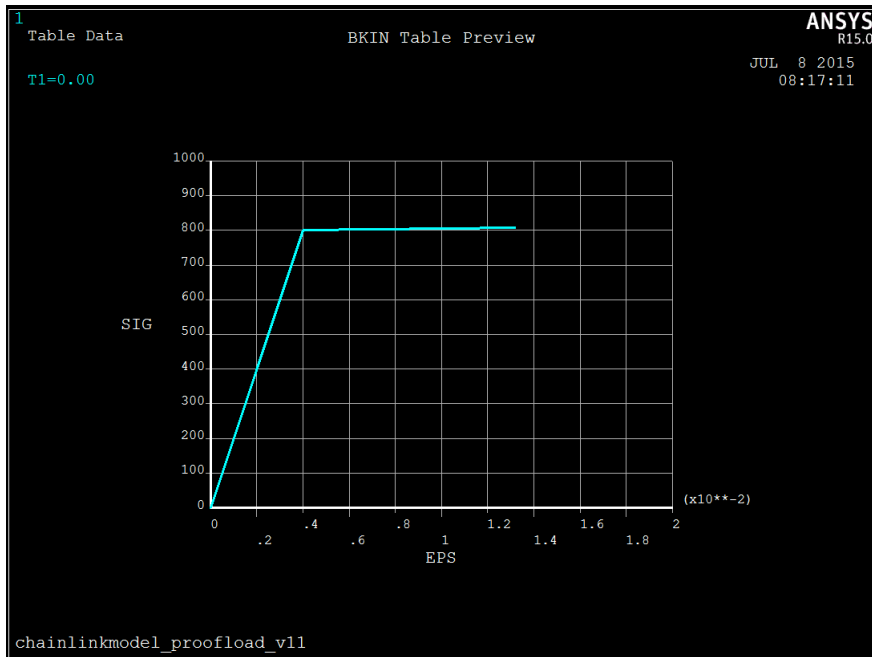


Figure 6.7: Bilinear kinematic hardening curve

This is important for the chainlink, since the surface deformation that will result in the interlocking of the links is caused by plastic deformation. It is thus

essential to take plasticity into account. As plasticity is a non-linear process, the simulation must be performed with non-linear capabilities. In the Ansys jargon, *large deformations* should be allowed.

It should be noted that geometrical non-linearity is not the only source of non-linear behaviour, the contact modeling is inherently nonlinear, as the contact *status* changes for different (sub)steps.

Ansys employs the so-called *Newton-Rhapson* method to be able to solve nonlinear simulations. The essence of this method is the division of the load in a number of load increments. For each load increment, Ansys performs a linear solution using the difference between (element) stresses and the applied loads, until convergence is reached. If the solution fails to converge, Ansys tries again with smaller load increments. The load increments and substeps are visualized in Figure 6.8.

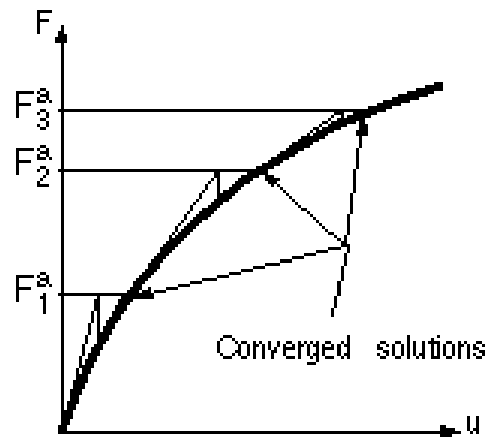


Figure 6.8: Newton-Rhapson concept. [Ansys, 2015]

6.2.3 Limitations

The finite element method is in essence a numerical approximation of the real situation. This means that there will always be an inherent deviation from the real result. However, when one chooses a sufficiently fine mesh, the results are of good enough quality for engineering and/or research purposes.

6.3 Analysis results

This section contains the FE analysis' results. As it would be too much to go into the complete results here, this chapter can be considered a summary, highlighting some important results and/or concepts.

6.3.1 Deformation, stresses & strain

As the chainlinks are loaded until 80% of the maximum breaking load, as is standard, the links enter the plastic phase of the stress-strain curve. This means that the deformation is permanent, as can be seen in Figure 6.9. This deformation is quite significant, as can be seen in the figure.

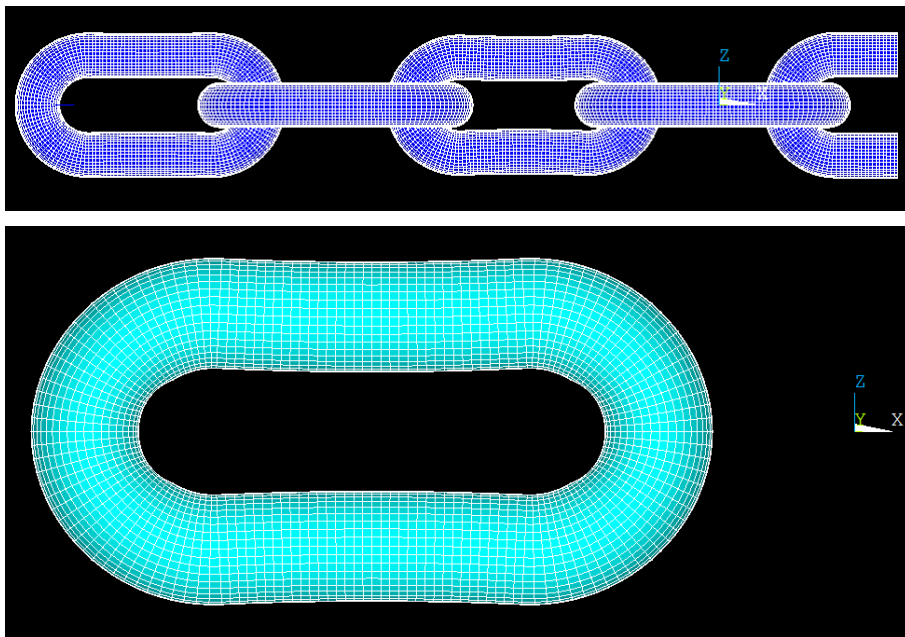


Figure 6.9: The chain shape after the proofloading step. A permanent deformation of the middle link is visible, in more detail in the bottom picture

When looking at the equivalent strain, as presented in Figure 6.10, it is clear how the links have deformed.

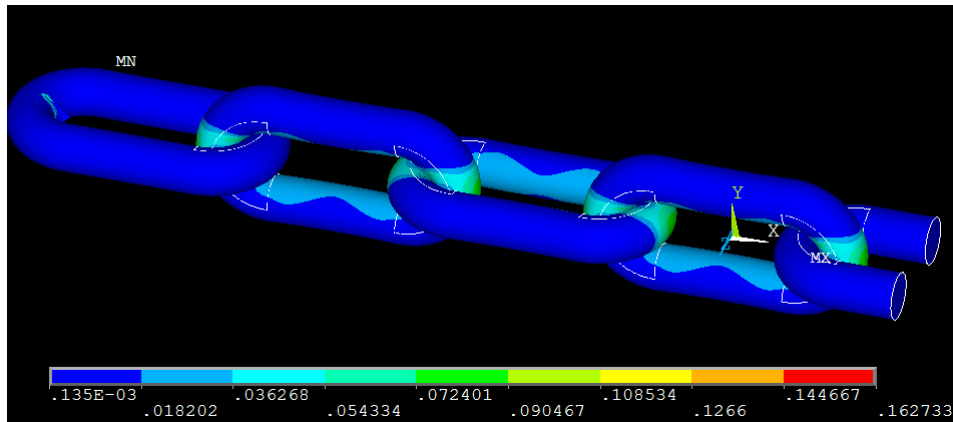


Figure 6.10: The strain during/after the proofloading

After the proofloading is completed and the links have deformed, the second phase of simulations can commence. In this phase, the material properties are fully elastic for all links. However, the geometry is updated to be the deformed geometry, which is essential for the out-of-plane bending problem, as was explained before. The chain will now be loaded with operational loads, while being given an offset from the purely tensional orientation.

In Figure 6.11 the stress intensity is plotted for the second loadstep, where no transverse translation is imposed on the links. However, already in this step there is a hint of the out-of-plane bending problem; there is already a clear spot of higher stress visible at the location right before the bend, outside the contact area. This is the location where the deformation had part of its effect, and where both the in-plane and out-of-plane bending will produce a stress-hotspot. Therefore, this location will be the focus of the simulation and the subsequent fatigue calculations.

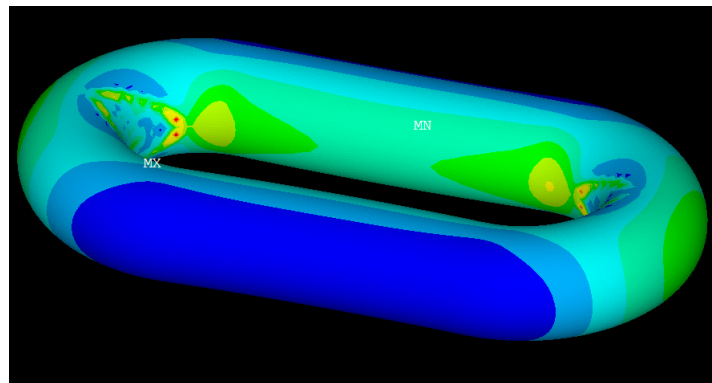


Figure 6.11: Stress intensity. Please note that in this particular plot, no bending is induced.

In Figure 6.12, the lower chainlink of Figure 6.5 is given an offset. The

result is a stress hotspot on the right part of the chain, introduced by both the in-plane and out-of-plane offset. Some stress time history plots have been added in Appendix C.

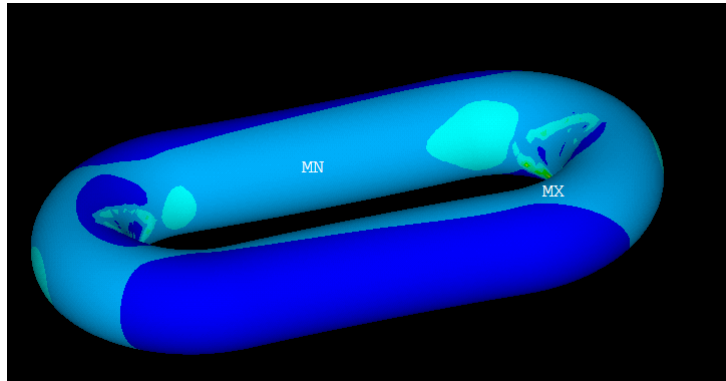


Figure 6.12: Stress intensity. In this loadstep, bending is induced by the offset of the lower chainlink

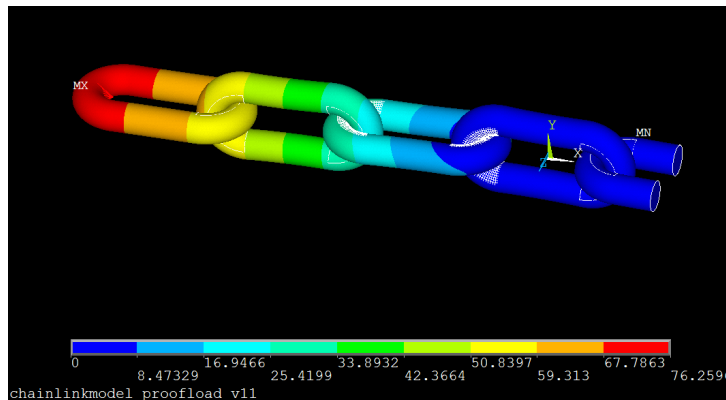


Figure 6.13: Displacement vector plot

When focusing on the OPB locations, there where the in-plane and out-of-plane stresses take hold, the spot is particularly visible, as can be seen in Figure 6.15. These locations will be input in the fatigue calculations. These locations can be seen again in Figures 6.16, 6.17 and 6.18, taken from [Golisz, 2015] and [Fernandez, 2008].

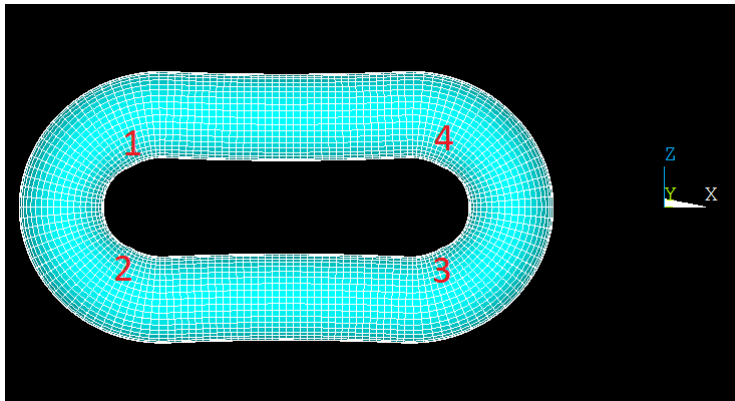


Figure 6.14: The four locations of interest

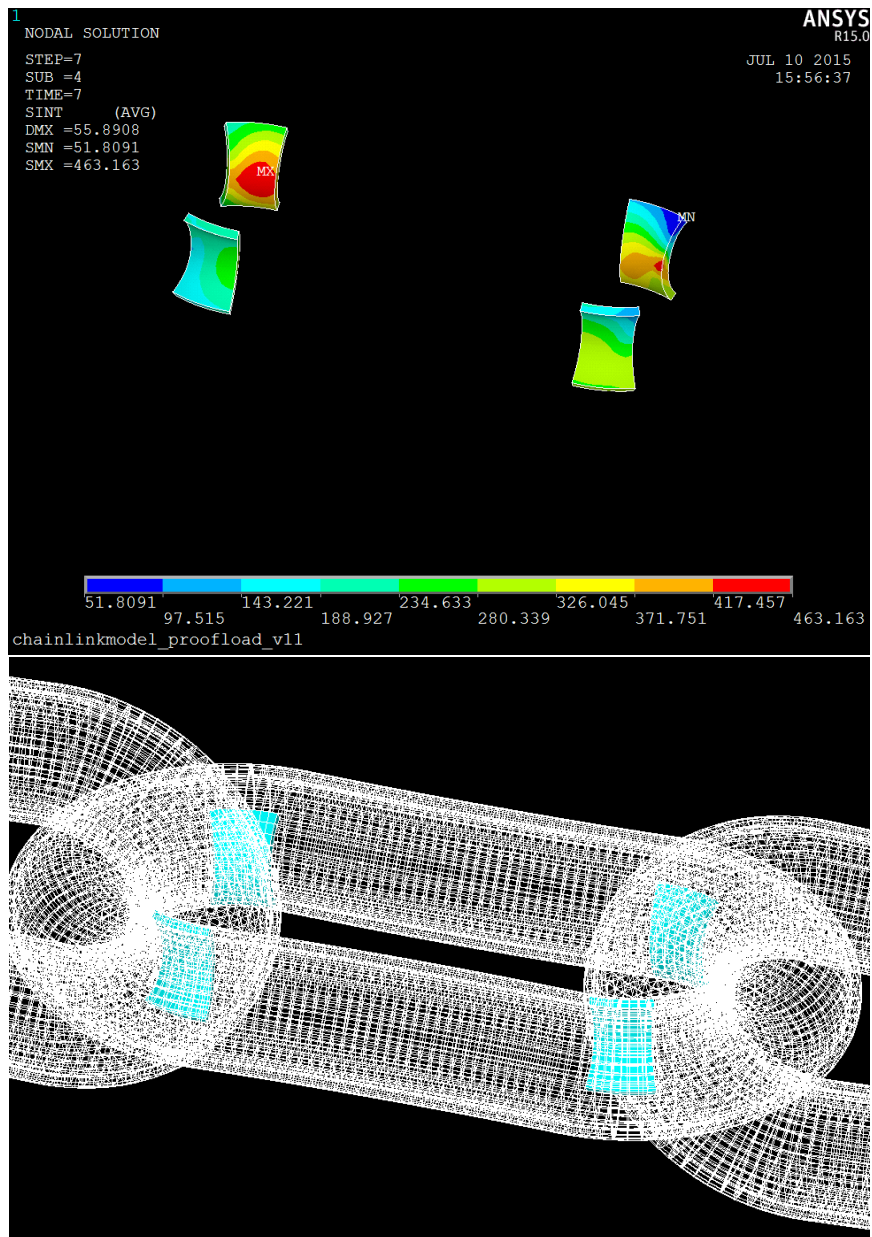


Figure 6.15: The four locations of interest, with stress distribution(top), in context (bottom)

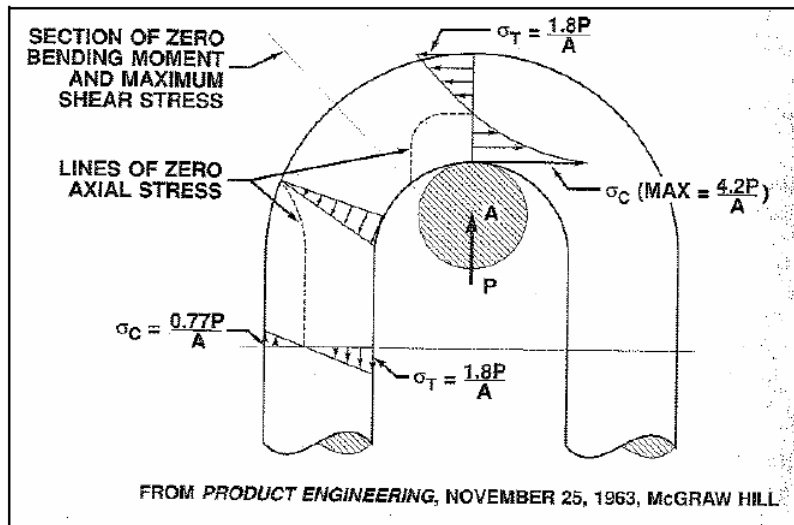


Figure 3-36 – Approximation of the Stress Distribution in a Typical Chain Link

Figure 6.16: The (approximate) stress distribution in the chain



Figure 6.17: The fracture location on a chain link [Fernandez, 2008]



Figure 6.18: The fracture locations on the link, from different angles [Fernandez, 2008]

7. Fatigue Analysis

This chapter presents the results of the fatigue calculations which were performed using the Pragtic software. The fatigue criteria either result in a Fatigue Index, which essentially states whether there is fatigue failure or not. The Dang Van criterion proposed by Burea Veritas' rules is of this kind. This method takes no cycle counting effects into account, as the maximum load is used.

The other kind of fatigue criteria result in a fatigue damage. This damage is the accumulated damage by the loading cycle. With a probability of occurrence of this cycle, life time predictions could be done. For lifetime predictions, a cycle counting method is performed, as not every point in the loading cycle is equally damaging. Different cycle counting options are possible in Pragtic.

7.1 Critical plane criterion

The definition of what defines the critical plane can be done according to multiple definitions. Most damage criteria discussed in this report are of the maximum damage kind; the plane that experiences the maximum damage according to the damage criterion is deemed the critical plane. When one accepts this formulation for the critical plane definition, one must also ask the question how to search for this critical plane. Mathematically speaking, there are infinitely many critical planes within the material. This of course poses a computational problem, because it is impossible to calculate infinitely many possible planes. In the theory at the beginning of this report, one plane search method has already been discussed, the Bannantine & Socie method.

7.1.1 Bannantine & Socie

The method acknowledges that the stress state on the free surface is a plane stress state. Then a specified number of planes will be investigated, each plane at an inclination from the normal to the free surface. This inclination can either correspond to a normal plane, a shear plane, or a combination. The planes are then calculated with the damage criterion. For a maximum damage criterion (MD), the plane experiencing the maximum damage is the critical plane. This can be a normal plane, but might as well be a shear or some differently oriented plane.

The fact that a limited number of planes is examined, inherently introduces some form of approximating the real plane. However, in [Socie and Marquis, 2000] it is claimed that an increment of 20° will only introduce a 20% error in estimated fatigue life.

The Bannantine & Socie method is the most efficient method, examining less planes, hence making it less computationally intensive.

7.1.2 Globe approach

To see to what extent the Bannantine & Socie method influences results, a number of criteria have been tested by using the *globe search method*. This method will be shortly explained in due course, but it can already be said that it is less

computationally efficient. Therefore, this method has only been examined for two locations on the link. A more elaborate look into differences between these methods would be enlightening, but this falls outside of the scope of this project. The globe analogy was implemented in Pragtic, and works as follows [Papuga, 2007]. Two coordinate systems are introduced, one begin the local coordinate system with one axis being normal to the surface of the examined point. The second coordinate system is obtained by two Euler angles. One of the axes of the second coordinate system corresponds to the normal line to the currently evaluated plane. This latter plane is a possible critical plane. Since two Euler angles are incremented, the normal lines to the possible planes describe meridians along a globe; hence the name. [Papuga, 2007] attempts to clarify with an illustration, see Figure 7.1. In this figure, the p-coordinate system is the local system, while the r-system is the one obtained after rotating the system according to the Euler angles ψ and ϕ . The r_3 axis is the line normal to the critical plane surface that is being examined.

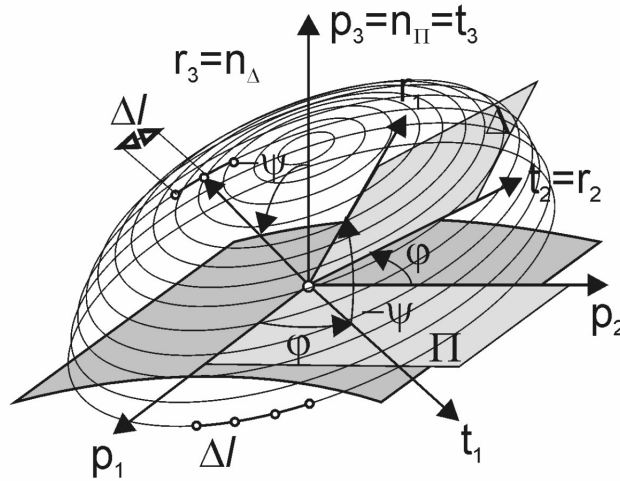


Figure 7.1: Globe concept [Papuga, 2007]

7.2 Fatigue calculations

The fatigue calculations' results are divided in two categories, being *Fatigue Index* (FI) and *Fatigue Damage* (FD). The examined FI criteria are: McDiarmid (two different formulations), Findley, Matake, Liu & Mahadevan, Dang Van and Carpinteri & Spagnoli (MD variant), the latter with a Smith, Watson & Topper mean stress formulation. The C&S criterion is implemented following the maximum damage concept, as the weight function of the original method uses a parameter of which it is uncertain whether or not applicable to the present material.

On the FD side, Wang & Brown (& Miller), Socie (shear method) and Smith, Watson & Topper are calculated.

Where applicable, the two cycle counting methods used are Wang & Brown or a rainflow count (on the shear variable). For FI criteria no cycle counting

methods are used. As these methods only predict failure or no failure, they use the maximum loading value in the cycle. No (accumulated) damage is calculated.

All results are presented graphically in Figure 7.2 to 7.7. On the horizontal axis, the location is presented, on the vertical axis either the Fatigue Index or the Fatigue Damage. The locations were specified in Figure 6.14. Names and abbreviations are specified in Table 7.1.

7.2.1 Fatigue Index

From the Fatigue Indices for Case 1, plotted in 7.2, a few observations can be made. Locations 3 and 4 are experiencing most damage. These are the locations adjacent to the fully constraint link; the locations closest to the top section of the chain. As the chain link it is 'locked' with cannot move freely, stresses in this part of the chain are higher than in the other two locations. At those locations (L1 and L2), the adjacent (lower) link is free to move.

Furthermore, there are virtually no differences between either L1 and L2 or between L3 and L4. This is expected, as the chain is only moved in one direction, normal to the plane of the examined chain link. Due to symmetry, there should be no difference between the locations on the same end of the link. Very small differences can however be observed, but the order of magnitude is very low. For instance, the Fatigue Index of the Dang Van criterion differs by about 0.003 between L3 and L4. This comes down to a difference of 0.6%. This negligible difference might be due to some small local geometrical differences, leading to small differences in the stress at both locations.

For all locations, the Dang Van criterion gives the lowest Fatigue Index, while the McDiarmid criterion gives the highest. It must be noted at this point that two different versions of the McDiarmid criterion have been calculated, namely a 1972 variant and a variant proposed in 1991 (which is the one described in the theory review, 4.1.3). The validity of the '72 variant is widely disputed, while the '91 version could count on slightly more support [Papuga, 2007].

The Carpinteri & Spagnoli criterion gives the second largest indices of all criteria. This criterion takes the mean stress into account, which in this particular case, could indeed be quite an important aspect. The values of the Mataka, McDiarmid '91, Findley and Liu & Mahadevan criteria are approximately equal to each other, it turns out.

| Method | Abbreviation |
|-----------------------|--------------|
| McDiarmid v. '72 | MCD |
| McDiarmid v. '92 | MCD91 |
| Mataka | Mataka |
| Liu & Mahadevan | LM |
| Caprinteri & Spagnoli | CS |
| Findley | Findley |
| Wang & Brown | WB |
| Smith, Watson, Topper | SWT |

Table 7.1: Abbreviations in plot legend

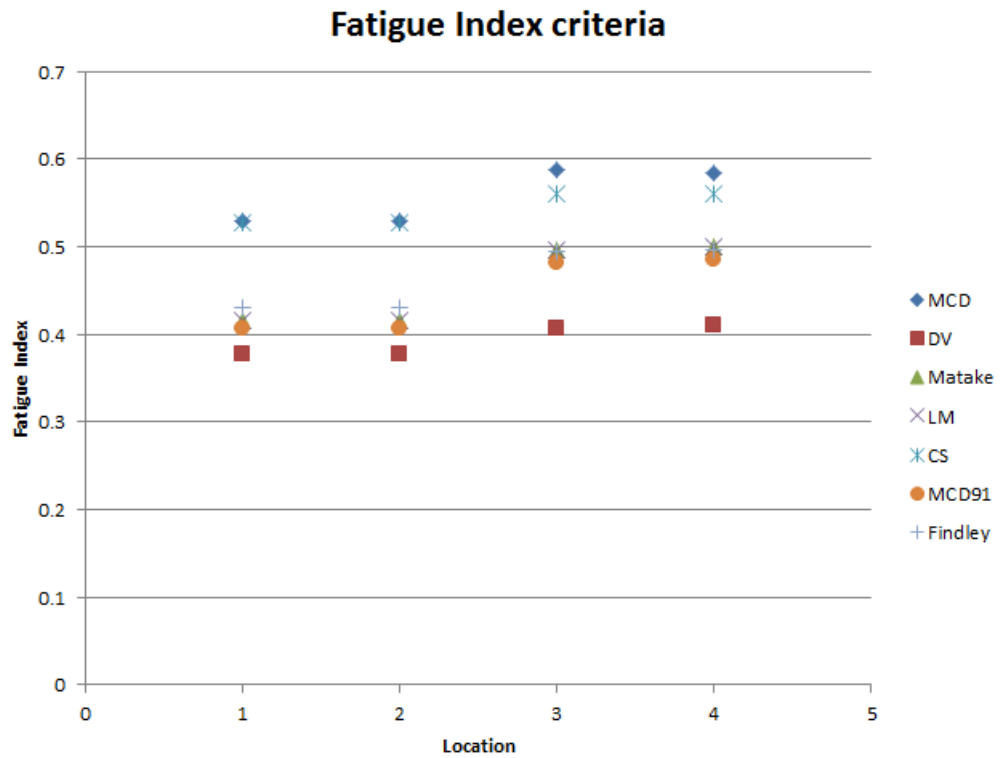


Figure 7.2: Case 1 Fatigue Indices

Now, the same criteria are calculated for Case 2, where the chain is moved both in and out-of-plane, as was shown in Figure 6.2. This extra angular effect has only a small effect on L1 and L2, but is especially noticeable at L3 and L4. The Fatigue Index is actually higher than one, which indicates the onset of fatigue cracks. As all examined criteria, apart from Findley, cross the threshold of 1, it seems to indicate that taking both angles into account can actually lead to safer fatigue predictions. The author stresses the use of the words *seems to indicate*, as ultimately experiments should validate this statement.

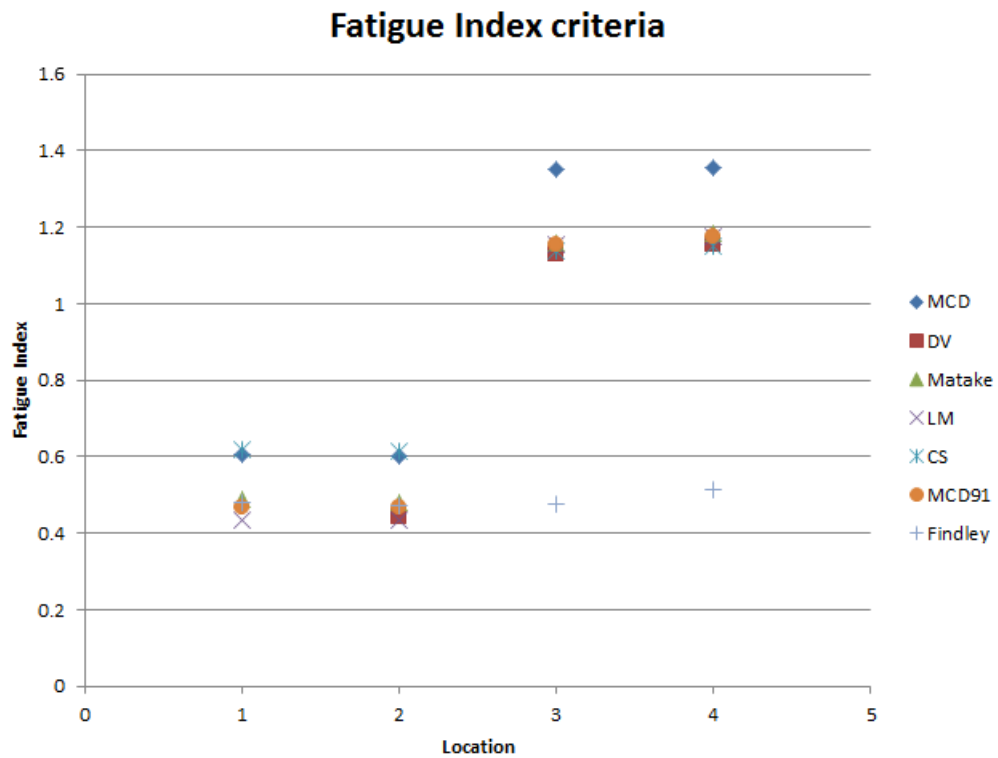


Figure 7.3: Case 2 Fatigue Indices

For Case 3 the imposed angles are out-of-phase. Compared to the results for Case 2, the effect of this loadcase, are fairly similar, see Figure 7.4. For some criteria, it can be seen that the Fatigue Index slightly lowers. This might be due to the fact that the maximum angles do not occur at the same instance, lowering the combined maximum stress. However, all indices are still higher than for Case 1, again stressing the need to take two angles into account. Furthermore, the capabilities of criteria to take a wide range of non-proportional effects into account is not always clear. Even for criteria that are supposedly valid for non-proportional loading, it is not said that it can be extended to complex problems, such as the problem investigated in this report. Sadly, the duration and costs of fatigue experiments, have lead to limited availability of data-sets for fatigue research, introducing some uncertainty with respect to validity ranges. Having said that, the fact that the usual uniaxial methods have been replaced by a multiaxial critical plane approach, should already be a significant step forward.

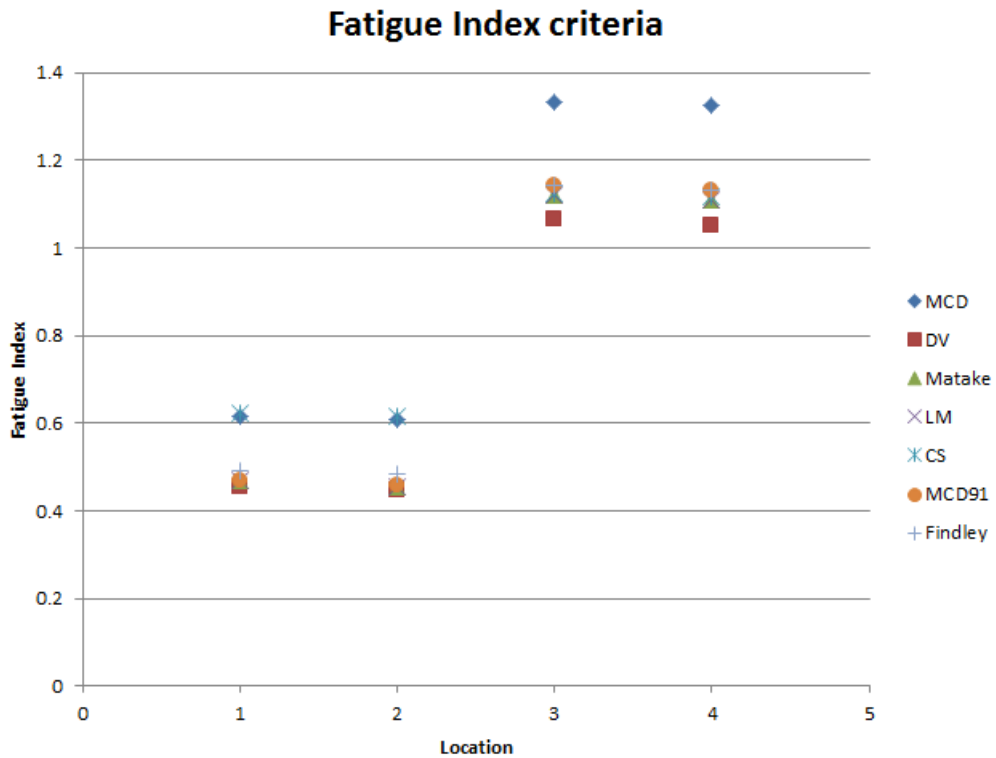


Figure 7.4: Case 3 Fatigue Indices

7.2.2 Fatigue damage

In this section the criteria that predict the accumulated damage are presented. Six criteria are discussed, namely Wang & Brown (WB96), Wang & Brown & Miller (WB93), Socie's shear method and Smith, Watson & Topper (SWT). Both WB93 and SWT are calculated using two different approaches regarding the cycle decomposition. WB93.1 implements the Wang & Brown method, while WB93.2 makes use of a rainflow on the shear stresses. The difference between the WB96 and the WB93 method is that WB93 implements the original proposal for looking for the plane with the maximum shear range. WB96 searches for the maximum damage instead. SWT_wb makes use of the Wang & Brown method, while SWT_vmred makes use of a signed Von Mises reduction of the shear variable. As mentioned before, SWT is originally a uniaxial criterion, but nonetheless often comes up in multiaxial literature. It is included here to see if this criterion shows some agreement with more multiaxial oriented methods, or should possibly be omitted from these calculations. Furthermore, the different cycle counting methods are implemented to see the extent of the influence of the choice of the method. Results are presented graphically in Figure 7.5 to 7.7. Please note that the vertical axes of these plots are logarithmic, making them somewhat better readable.

Accumulated Damage Criteria

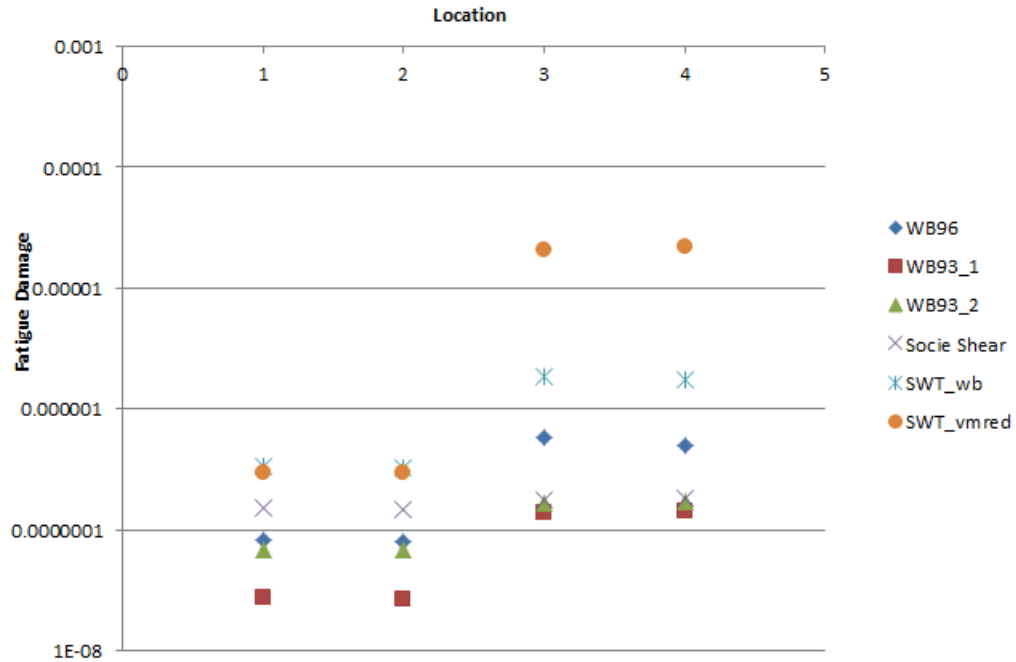


Figure 7.5: Case 1 Fatigue Damage

First thing that stands out in Figure 7.5, is that the SWT criteria give the highest damage. However, for Case 3 (Figure 7.7, SWT_vmred gives the lowest damage at L3 and L4. This leads to the believe that this method overestimates the damage for Case 1 and Case 2, but underestimates it for Case 3. For Case 3, the loading angles are out-of-phase, which can lead to locally lower instantaneous stress components. As SWT is uniaxial, a lower stress might lower the damage, while the effects of other stress components are ignored. This can go the other way around, too, if the uniaxial stress component is high, while other components are not incorporated, the damage might be too high. Wang & Brown's method (WB96) is more consistent throughout the cases and the most conservative (ignoring SWT). Furthermore, the difference between WB96, WB93 and Socie method are generally very modest. For Case 1, Socie's method does not show much of a difference between locations. However, for Case 2 and Case 3, the difference between the L1/L2 and L3/L4 is more pronounced. This is due to the fact that the shear stresses between the two groups differs much more when taking two angles into account.

Finally, to give some idea of the damage translated to a timescale, for the WB96 method, the damages would lead to failure in approximately 390 days for Case 1, and about 19 days for Case 3. This is of course a massive difference and shows how detrimental the combination of the angles is. Before assuming that all chains around the world will fail within the next two weeks, it should be

noted that the imposed angular range of 10° is quite large and will not occur constantly for days in a row. It can be seen as sort of a worst case scenario. To make a proper estimate of the time to failure, probabilities of sea-states and consequently the angular range distribution need to be taken into account. This will give a more realistic approximation of the fatigue life.

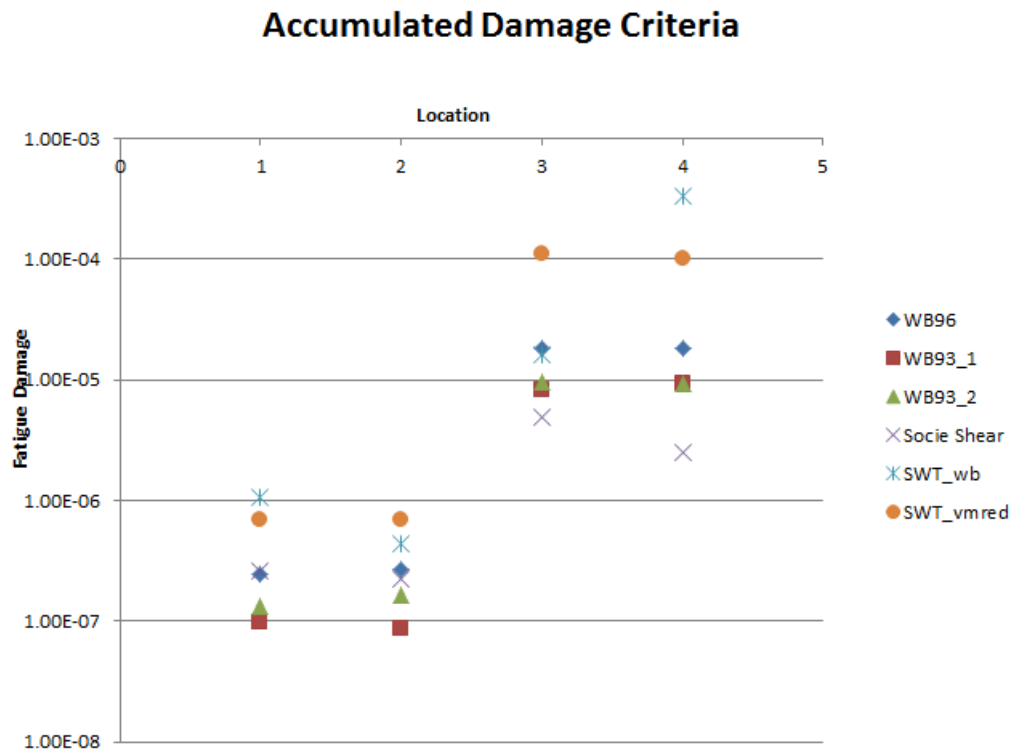


Figure 7.6: Case 2 Fatigue Damage

Accumulated Damage Criteria

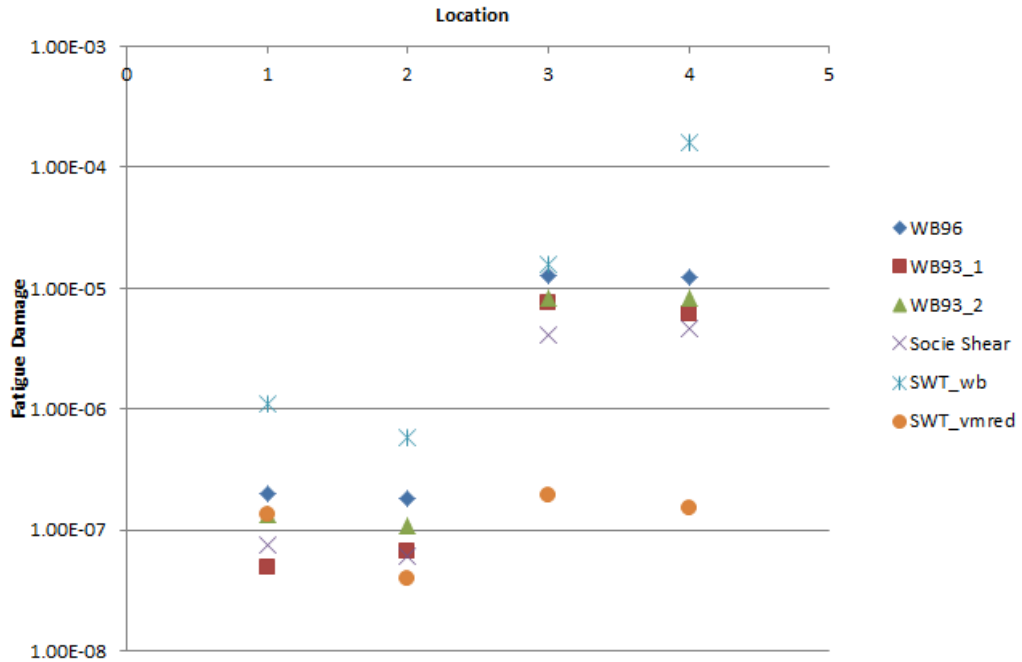


Figure 7.7: Case 3 Fatigue Damage

7.2.2.1 Critical plane orientation

The critical plane is defined by the angle between the normal to the free surface and the normal to the critical plane. The orientation of the plane might help shedding some light on the mechanisms that are more damaging, and can ultimately lead to failure. However, by definition, the critical plane is dependent on the used damage criterion. This means that the orientations calculated are somewhat subjective, since it gives no information on the validity of the damage criterion itself. But, since a large number of methods are examined, some trends can be discovered, to lead to a general statement that will need more validation by means of experiments.

In Figure 7.8 to 7.10 it can be seen that the orientations are basically either 45° or 90° , as expected from the Bannantine and Socie method. With regards to the most damaged locations, L3 and L4, the general trend seems to be an angle of 45° , for Case 1. This essentially suggests that the critical plane is (close) to a shear plane, for purely out of plane excitation.

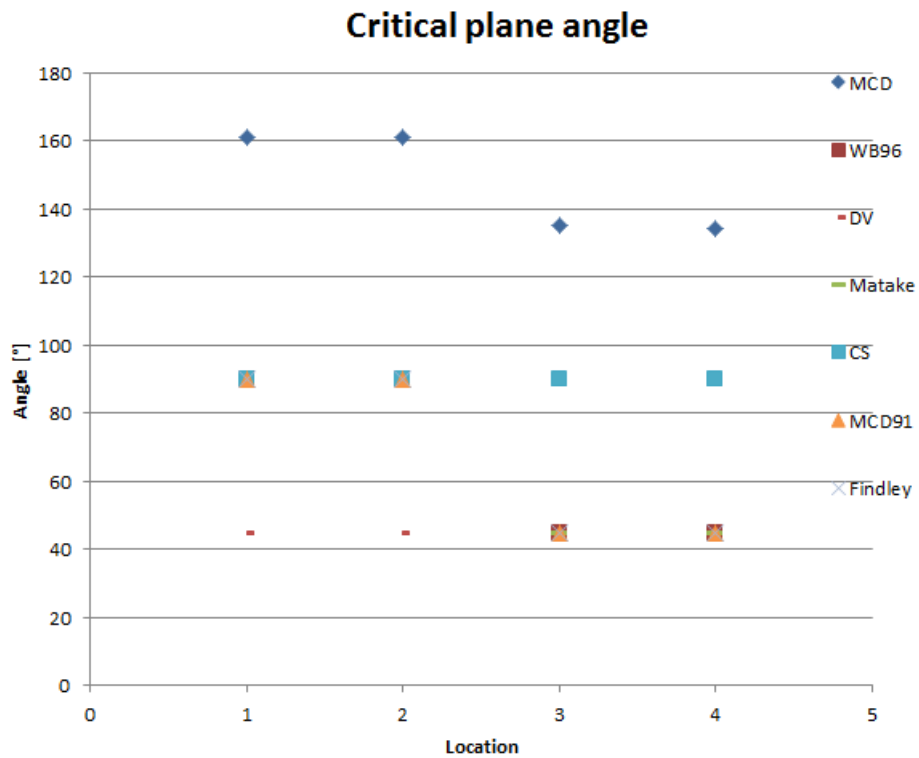


Figure 7.8: Case 1 Critical plane orientation; the angle is the angle between normal to the free surface and normal to critical plane

For Case 2 and Case 3, Figure 7.9 and 7.10, a trend is less pronounced. This is not entirely unexpected, as the loading is more complex. While the out-of-plane angle might 'create' a shear critical plane, the in-plane excitation angle can form a normal plane, due to the in-plane tension that occurs as a consequence of the locking of the links. For Case 3, the WB96 method, it stands out that the plane orientation differs for L3 and L4. Due to the two angles being out-of-phase with each other, the magnitude and orientation of the stresses differ between these two locations, leading to different critical planes.

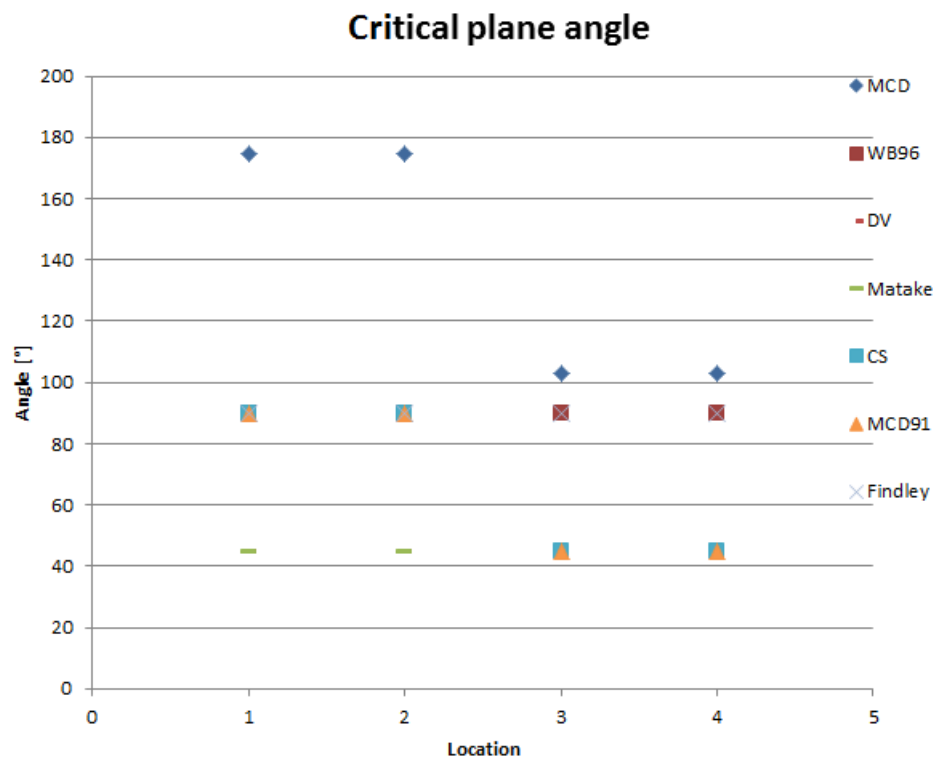


Figure 7.9: Case 2 Critical plane orientation; the angle is the angle between normal to the free surface and normal to critical plane

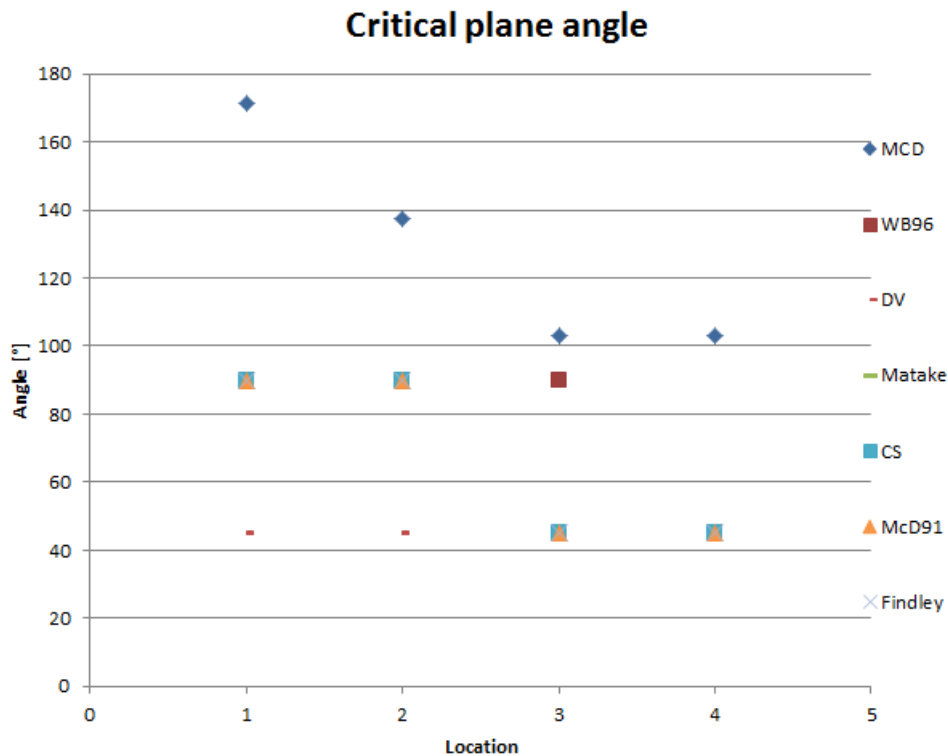


Figure 7.10: Case 3 Critical plane orientation; the angle is the angle between normal to the free surface and normal to critical plane

7.2.3 Globe concept

This section shows the results for calculations done with another critical plane search criterion, namely the globe search concept, see section 7.1.2. Due to the method being more computationally intensive, only two locations on the link have been examined for Case 1 and Case 3. A more complete investigation into critical plane search algorithms was deemed to fall outside of the scope of this project. This section is intended to raise some awareness of possible influencing factors for the damage criteria, but is far from a complete critical examination of critical plane search concepts.

As can be seen from Figures 7.11 to 7.14, there is not a great difference between the calculated damage criteria. There is a slight tendency to the globe approach being slightly more damaging. The reason that this is the case, is that the globe approach investigates more critical plane orientations. Whereas the Bannantine & Socie method examines the normal and shear planes, the globe concept search along a more general route. This leads to a possibility to find a slightly more damaging plane, which is still relatively close to the plane found with Bannantine & Socie. For instance, let us examine the Findley method at L3 for Case 3. The B&S method gives a critical plane orientation of 45° with a damage of ~ 1.13. The globe search, for the same location, case and method, gives a critical plane

orientation of 55° with a damage of ~ 1.19 . These damages lie at $\sim 5\%$ of each other. The critical plane is thus not a pure shear plane, but a plane close to that. So, for a more detailed approximation of the critical plane orientation, the globe concept might be more suitable. This does, like everything in life, come at a cost, as the globe concept is computationally more intensive. As for the damages, they are fairly similar, so for general design purposes B&S should be sufficient.

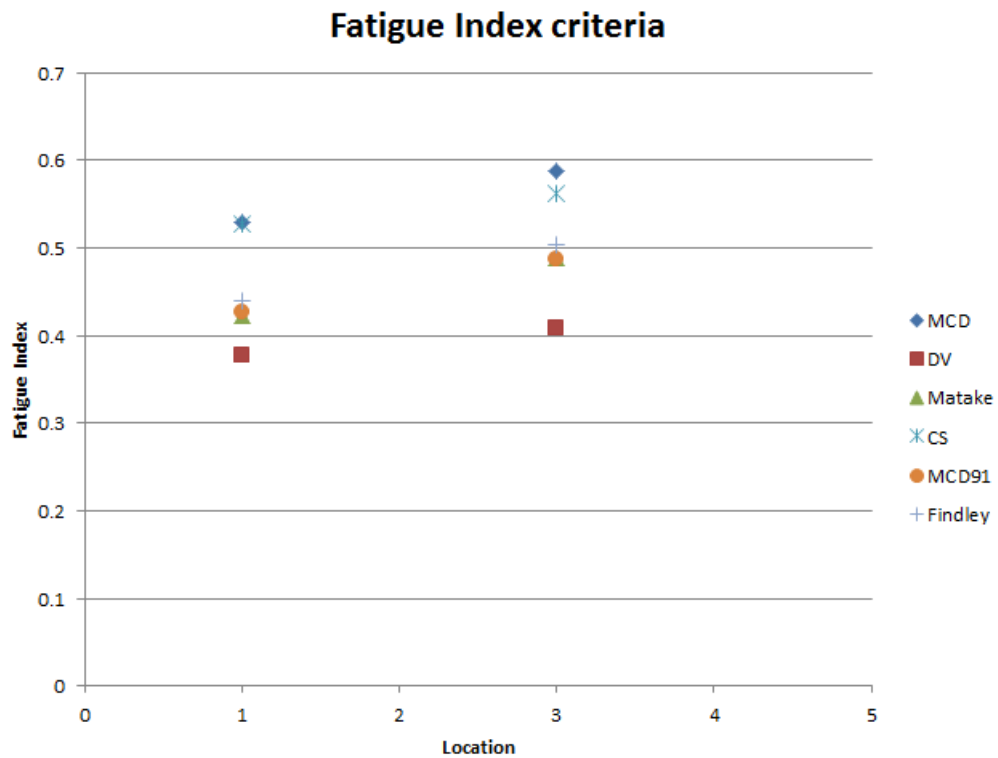


Figure 7.11: Case 1 Fatigue Indices Globe Concept

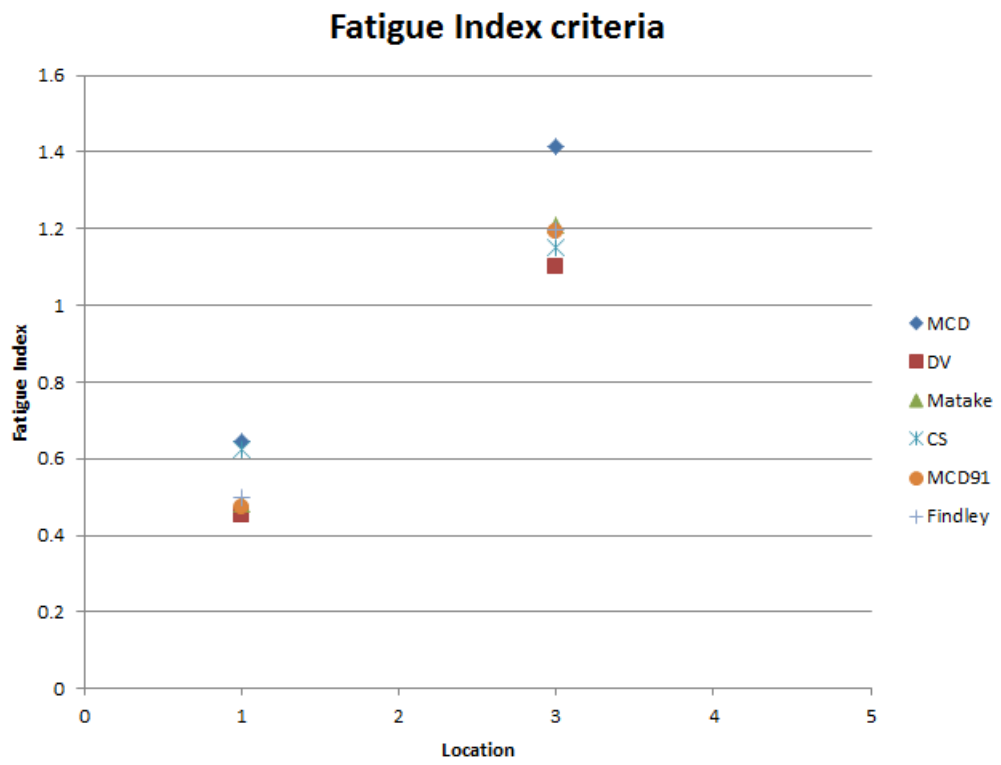


Figure 7.12: Case 3 Fatigue Indices Globe Concept

Accumulated Damage Criteria

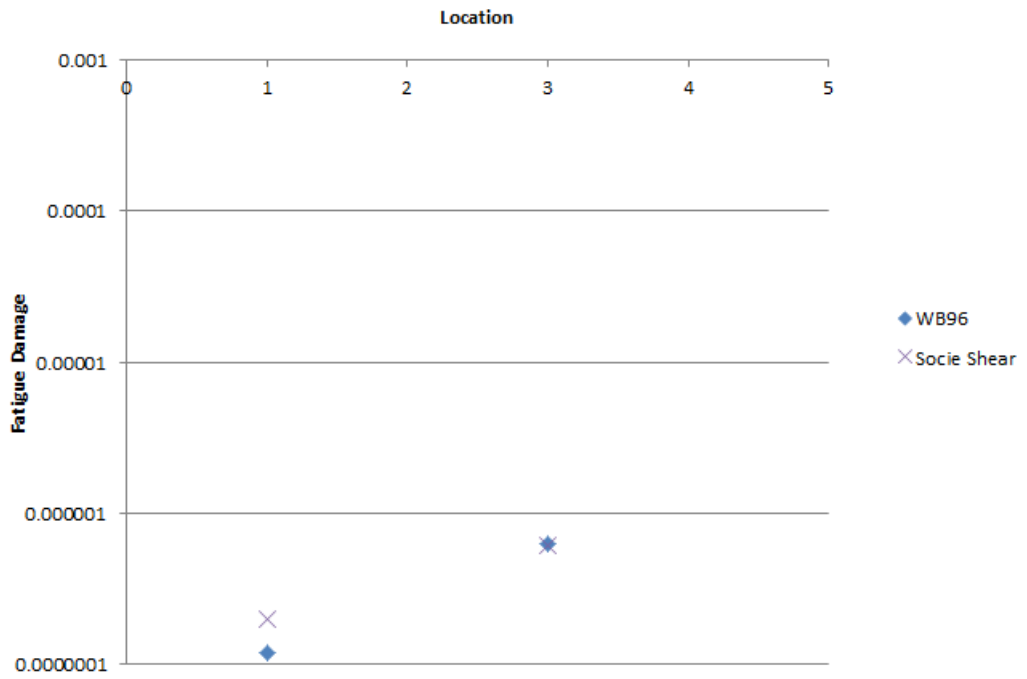


Figure 7.13: Case 1 Fatigue Damage Globe Concept

Accumulated Damage Criteria



Figure 7.14: Case 3 Fatigue Damage Globe Concept

8. Conclusions

This report set out to compare a number of fatigue criteria for the fatigue calculations of offshore mooring chains. The intention was to attribute this work towards a more complete fatigue calculation method for mooring chains subjected to out-of-plane bending. From the results, a number of conclusions can be drawn.

For the case of a purely out-of-plane excitation angle, all criteria show similar behaviour and values. It seems that basically any multiaxial criterion is as good as the other, with some minor differences. With respect to the Fatigue Index criteria, the Dang Van criterion is on the lower end of the spectrum. As this criterion is mentioned in BV's rules for out-of-plane bending of mooring chains, it could be important to note that this criterion is slightly less conservative with respect to other criteria. For the Fatigue Damage concepts, the Wang&Brown method yields most damage, when dismissing the uniaxial approach of Smith, Watson and Topper. The WB method incorporates a multiaxial (non-proportional) cycle counting method.

For Case 2 and 3, the chain was also excited with an in-plane angle. For Case 2 both angles are in-phase, while for Case 3 they are out-of-phase. For both Case 2 and Case 3, the Fatigue Indices and/or damages are significantly higher. This leads to the notion that it is important to simultaneously implement both angles, in order to realistically assess the damage on the mooring chain.

For the locations experiencing the most damage under a purely out-of-plane excitation, the material plane experiencing the most damage is (close to) the shear plane, according to most criteria. However, as the loading gets more complex for Case 2 and Case 3, the critical plane orientations are more divided over the normal and shear plane. In other words, the tendency of the shear plane being the most damaged is less pronounced. When investigating more possible planes using the globe concept, it was observed that a number of methods actually show more damage on planes somewhere inbetween shear and normal planes. In some sense, this feels intuitive, that the plane experiencing the maximum damage does not show a pronounced inclination towards one stress state. Instead the critical plane is located on a location where the combination of the stress state induced damage takes a maximum, which feels more in accordance with the maximum damage concept.

The complex nature of the loading and resulting stresses and strain fuel the need to use multiaxial approaches to properly assess the fatigue damage. The critical plane maximum damage seems the method that is both capable of taking a range of effects into account, while still being fairly easy to implement. From the obtained results, it is hard to put one criterion before the other. The Wang & Brown method seems to be fairly conservative, while it does take mean stress and multiaxial cycle counting into account. It therefore seems likely that this is a more useful criterion. However, the author will remain cautious upon making such claims, since ultimately, fatigue experiments must put these statements to the test.

As for locations on the link to be examined, it seems clear from the results, that the two locations that matter most are the locations closest to the fully constraint adjacent link. This is in accordance with observations [Jean et al., 2005].

9. Discussion & Recommendations

The OPB problem for mooring chains is quite a complex problem. To fully explore fatigue properties, more model tests need to be performed. This will help get rid of uncertainties in fatigue properties of the mooring chain (material). As much data on mooring line material properties is the result of expensive fatigue tests, test results are not easily obtainable. It should be noted here that Vicinay has kindly provided some limited information, which led to being able to make some reasonable approximations. Some parameters have been approximated with a rule of thumb, or from materials with similar properties and/or heat treatments. To be fully able to work out fatigue criteria, these parameters need to be specified for the exact chain material and for different types of loading. Even more so, a greater amount of data, might enable the formulation of a completely new fatigue criterion.

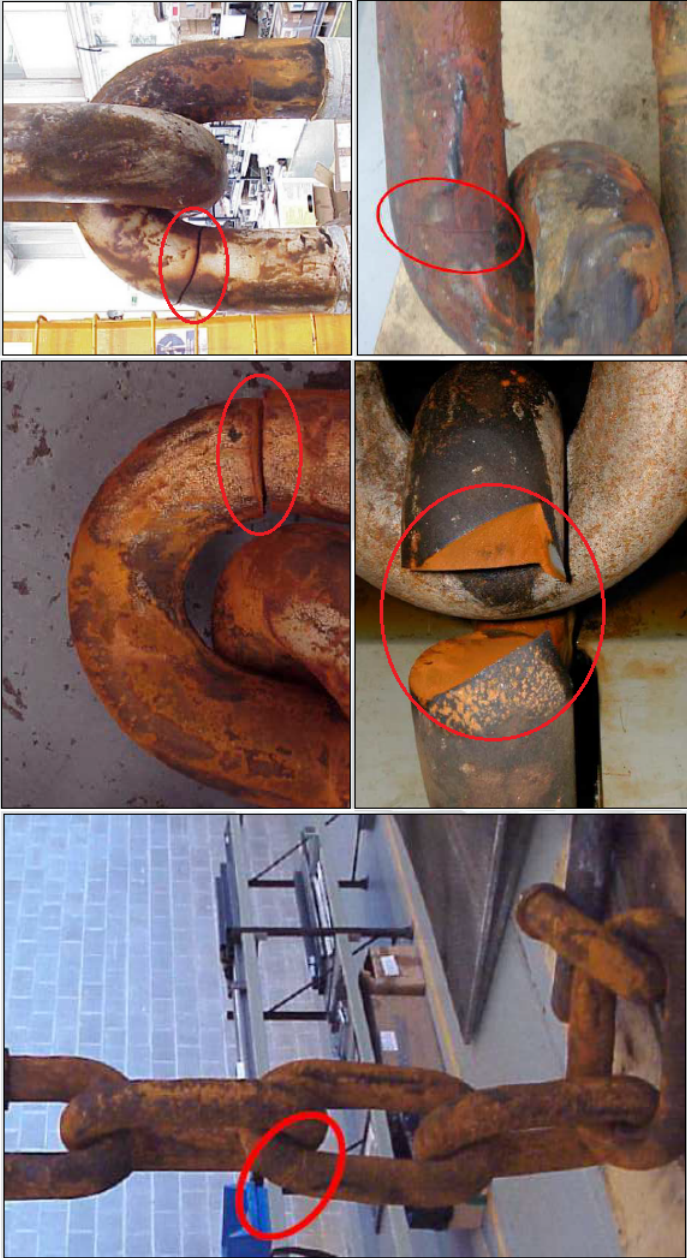
More directly linked to this work, a wider range of cases should be examined. When exploring more angle ranges and phase differences, a more complete picture of the resulting stress/strain effects can be obtained. To make the simulation even more realistic, the axial tension might also be given a fluctuation. This could be a simple cosine, but could also be some probabilistic distribution, which can be closely related to the wave height distribution. Also, it might be interesting to add some torsion to the chainlink, to arrive at a complex, but complete exploration of different loading effects that can occur. These steps should be relatively easy to implement, but the running of the simulations and subsequent result processing might take up a considerable amount of time. Furthermore, the amount of fatigue criteria existing is quite extensive. Some are better tried and tested than others, but a more unabridged exploration of criteria is possible. The obtained data from both experiments and FEA could lead to finding the appropriate fatigue criterion, which can lead to better prediction methods. This research set out to do such a thing, but because of practical and time limits, can be considered merely as a few starting steps into this interesting and important field. A complete, fully comprehensive research project might take years and would therefore be likely to be performed by a PhD candidate, or a Joint Industry Project.

Also, it might be interesting to do some sensitivity studies into mesh size, different material properties, etc. Sensitivity analyses into different material (properties) and constants used in criteria might possibly provide even more insight in the parameters that govern the fatigue behaviour of mooring chains. This can obviate some uncertainty regarding the exact phenomena.

With regards to mesh size, a smaller mesh size might lead to large element distortion for the plastic part of the calculation, leading to convergence problems. These problems were already encountered for the present calculations, but could be overcome. Smaller mesh size might lead to more trouble overcoming these problems.

Appendices

A. Crack Locations



B. Pragtic

The Pragtic print screens presented here are mostly for illustrational purposes. If one would like to re-create some of the results, these print screens of the calculation methods might be of assistance. The approaches implemented have been discussed in the main body of the thesis, however.

| MCD | | | | | | | | | | | | | | | |
|--|------------------------|---------------------|-----------|--------------------------------------|--------|--|------|--------------------------|-----|-------------------------|-----|--|-----|--|---|
| WB96 WB93_1 WB93_2 FINDLEYS_WB FINDLEYS_SR FINDLEYS_MAX DV SOCSHEAR MATAKE LM CS SWT_WB SWT_VMRED MCD91 FINDLEYS | | | | | | | | | | | | | | | |
| ID-name: | MCD | | | | | | | | | | | | | | |
| Description: | | | | | | | | | | | | | | | |
| Method: | McDiarmid v.72 | | | | | | | | | | | | | | |
| Material: | 3 | | | | | | | | | | | | | | |
| Decomposition: | Whole load path | | | | | | | | | | | | | | |
| Elasto-plasticity: | No | | | | | | | | | | | | | | |
| Mean stress influence: | As in original formula | | | | | | | | | | | | | | |
| Influence of stress gradient: | No | | | | | | | | | | | | | | |
| Influence of technology: | No | | | | | | | | | | | | | | |
| Influence of surface quality: | No | | | | | | | | | | | | | | |
| Influence of size: | No | | | | | | | | | | | | | | |
| Influence of temperature: | No | | | | | | | | | | | | | | |
| Set another survive probability: | No | | | | | | | | | | | | | | |
| Cumulative rule: | No | | | | | | | | | | | | | | |
| <table border="1"> <thead> <tr> <th>Solution option</th> <th>Parameter</th> </tr> </thead> <tbody> <tr> <td>CP criterion <0~MD, 1~MSSR, 2~MMES ></td> <td>0</td> </tr> <tr> <td>Searched planes <0~BS, 1~globe, 2~random, 3~N only ></td> <td>1</td> </tr> <tr> <td>Number of scanned planes</td> <td>45</td> </tr> <tr> <td>Optimize <1~yes, 0~no ></td> <td>1</td> </tr> <tr> <td>Negative mean stress <0~zeroized, 1~used ></td> <td>0</td> </tr> <tr> <td>Only every x-th data-point taken from load history</td> <td>1</td> </tr> </tbody> </table> | | Solution option | Parameter | CP criterion <0~MD, 1~MSSR, 2~MMES > | 0 | Searched planes <0~BS, 1~globe, 2~random, 3~N only > | 1 | Number of scanned planes | 45 | Optimize <1~yes, 0~no > | 1 | Negative mean stress <0~zeroized, 1~used > | 0 | Only every x-th data-point taken from load history | 1 |
| Solution option | Parameter | | | | | | | | | | | | | | |
| CP criterion <0~MD, 1~MSSR, 2~MMES > | 0 | | | | | | | | | | | | | | |
| Searched planes <0~BS, 1~globe, 2~random, 3~N only > | 1 | | | | | | | | | | | | | | |
| Number of scanned planes | 45 | | | | | | | | | | | | | | |
| Optimize <1~yes, 0~no > | 1 | | | | | | | | | | | | | | |
| Negative mean stress <0~zeroized, 1~used > | 0 | | | | | | | | | | | | | | |
| Only every x-th data-point taken from load history | 1 | | | | | | | | | | | | | | |
| <table border="1"> <thead> <tr> <th>Material parameters</th> <th>Value</th> </tr> </thead> <tbody> <tr> <td>E</td> <td>200000</td> </tr> <tr> <td>NU</td> <td>0.3</td> </tr> <tr> <td>SIG_ULT</td> <td>860</td> </tr> <tr> <td>TENS-1</td> <td>430</td> </tr> <tr> <td>TORS-1</td> <td>250</td> </tr> </tbody> </table> | | Material parameters | Value | E | 200000 | NU | 0.3 | SIG_ULT | 860 | TENS-1 | 430 | TORS-1 | 250 | | |
| Material parameters | Value | | | | | | | | | | | | | | |
| E | 200000 | | | | | | | | | | | | | | |
| NU | 0.3 | | | | | | | | | | | | | | |
| SIG_ULT | 860 | | | | | | | | | | | | | | |
| TENS-1 | 430 | | | | | | | | | | | | | | |
| TORS-1 | 250 | | | | | | | | | | | | | | |
| <table border="0"> <tr> <td>Help</td> <td>Save</td> <td>New</td> <td>Remove</td> </tr> <tr> <td>Skip</td> <td>Copy</td> <td>Close</td> <td></td> </tr> </table> | | Help | Save | New | Remove | Skip | Copy | Close | | | | | | | |
| Help | Save | New | Remove | | | | | | | | | | | | |
| Skip | Copy | Close | | | | | | | | | | | | | |

MCD
WB96
WB93_1
WB93_2
FINDLEYS_WB
FINDLEYS_SR
FINDLEYS_MAX
DV
SOCSHEAR
MATAKE
LM
CS
SWT_WB
SWT_VMRED
MCD91
FINDLEYS

ID-name:

Description:

Method: Material:

Decomposition:

Elasto-plasticity:

Mean stress influence:

Influence of stress gradient:

Influence of technology:

Influence of surface quality:

Influence of size:

Influence of temperature:

Set another survive probability:

Cumulative rule:

| Material parameters | Value |
|---------------------|--------|
| E | 200000 |
| NU | 0.3 |
| SIG_UL | 860 |
| TORS-1A | 250 |
| TORS-1B | 250 |

| Solution option | Parameter |
|---|-----------|
| CP criterion <0~MD, 1~MSSR, 2~MMES> | 0 |
| Searched planes <0~BS, 1~globe, 2~random, 3~N only> | 1 |
| Number of scanned planes | 45 |
| Optimize <1~yes, 0~no> | 1 |
| Negative mean stress <0~zeroized, 1~used> | 0 |
| Only every x-th data-point taken from load history | 1 |

Help Save New Remove
Skip Copy Close

MCD
WB96
WB93_1
WB93_2
FINDLEYS_WB
FINDLEYS_SR
FINDLEYS_MAX
DV
SOCSHEAR
MATAKE
LM
CS
SWT_WB
SWT_VMRED
MCD91
FINDLEYS

ID-name:

Description:

Method: Material:

Decomposition:

Elasto-plasticity:

Mean stress influence:

Influence of stress gradient:

Influence of technology:

Influence of surface quality:

Influence of size:

Influence of temperature:

Set another survive probability:

Cumulative rule:

| Material parameters | Value |
|---------------------|--------|
| E | 200000 |
| NU | 0.3 |
| SIG_F | 1700 |
| EPS_F | 0.33 |
| EXP_B | -0.139 |
| EXP_C | -0.498 |
| K' | 2200 |
| N' | 0.272 |
| S_WB | 0.3 |
| NU_EFF | 0.3 |

| Solution option | Parameter |
|---|-----------|
| CP criterion <0~MD, 1~MSSR, 2~MMES> | 0 |
| Searched planes <0~BS, 1~globe, 2~random, 3~N only> | 1 |
| Number of scanned planes | 45 |
| Number of scanned directions on each plane | 18 |

| Solution variable | Value |
|----------------------------------|-------|
| Minimum damage | 1E-20 |
| Weight of non-closed half-cycles | 0.5 |

Help Save New Remove
Skip Copy Close

MCD
WB96
WB93_1
WB93_2
FINDLEYS_WB
FINDLEYS_SR
FINDLEYS_MAX
DV
SOCSHEAR
MATAKE
LM
CS
SWT_WB
SWT_VMRED
MCD91
FINDLEYS

ID-name: WB93_1

Description: wb cycle count

Method: WB 1993 Material: 3

Decomposition: Wang-Brown v.'96

Elasto-plasticity: No

Mean stress influence: As in original formula

Influence of stress gradient: No

Influence of technology: No

Influence of surface quality: No

Influence of size: No

Influence of temperature: No

Set another survive probability: No

Cumulative rule: Palmgren-Miner

| Material parameters | Value |
|---------------------|--------|
| E | 200000 |
| NU | 0.3 |
| SIG_F | 1700 |
| EPS_F | 0.33 |
| EXP_B | -0.139 |
| EXP_C | -0.498 |
| K' | 2200 |
| N' | 0.272 |
| S_WB | 0.3 |
| NU_PL | 0.3 |

| Solution option | Parameter |
|--|-----------|
| CP criterion <0~MD, 1~MSSR, 2~MMES > | 0 |
| Searched planes <0~BS, 1~globe, 2~random, 3~N only > | 1 |
| Number of scanned planes | 45 |
| Number of scanned directions on each plane | 18 |

| Solution variable | Value |
|----------------------------------|-------|
| Minimum damage | 1E-20 |
| Weight of non-closed half-cycles | 0.5 |

Help Save New Remove
Skip Copy Close

MCD
WB96
WB93_1
WB93_2
FINDLEYS_WB
FINDLEYS_SR
FINDLEYS_MAX
DV
SOCSHEAR
MATAKE
LM
CS
SWT_WB
SWT_VMRED
MCD91
FINDLEYS

ID-name: WB93_2

Description: shear resolved

Method: WB 1993 Material: 3

Decomposition: Rain-flow of resolved shear variable

Elasto-plasticity: No

Mean stress influence: As in original formula

Influence of stress gradient: No

Influence of technology: No

Influence of surface quality: No

Influence of size: No

Influence of temperature: No

Set another survive probability: No

Cumulative rule: Palmgren-Miner

| Material parameters | Value |
|---------------------|--------|
| E | 200000 |
| NU | 0.3 |
| SIG_F | 1700 |
| EPS_F | 0.33 |
| EXP_B | -0.139 |
| EXP_C | -0.498 |
| S_WB | 0.3 |
| NU_PL | 0.3 |

| Solution option | Parameter |
|--|-----------|
| CP criterion <0~MD, 1~MSSR, 2~MMES > | 0 |
| Searched planes <0~BS, 1~globe, 2~random, 3~N only > | 1 |
| Number of scanned planes | 45 |
| Number of scanned directions on each plane | 18 |

| Solution variable | Value |
|---|-------|
| Minimum damage | 1E-20 |
| Weight of non-closed half-cycles | 0.5 |
| Size of too small cycles (to be erased) | 0 |

Help Save New Remove
Skip Copy Close

ID-name:

Description:

Method: Material:

Decomposition:

Elasto-plasticity:

Mean stress influence:

Influence of stress gradient:

Influence of technology:

Influence of surface quality:

Influence of size:

Influence of temperature:

Set another survive probability:

Cumulative rule:

| Material parameters | Value |
|---------------------|--------|
| E | 200000 |
| NU | 0.3 |
| TENS-1 | 430 |
| TORS-1 | 250 |

| Solution option | Parameter |
|---|-----------|
| Searched planes <0~BS, 1~globe, 2~random, 3~N only> | 1 |
| Number of scanned planes | 45 |
| Optimize <1~yes, 0~no> | 1 |
| Negative mean stress <0~zeroized, 1~used> | 0 |
| Only every x-th data-point taken from load history | 1 |

MCD
WB96
WB93_1
WB93_2
FINDLEYS_WB
FINDLEYS_SR
FINDLEYS_MAX
DV
SOCSHEAR
MATAKE
LM
CS
SWT_WB
SWT_VMRED
MCD91
FINDLEYCS

ID-name:

Description:

Method: Material:

Decomposition:

Elasto-plasticity:

Mean stress influence:

Influence of stress gradient:

Influence of technology:

Influence of surface quality:

Influence of size:

Influence of temperature:

Set another survive probability:

Cumulative rule:

| Material parameters | Value |
|---------------------|--------|
| E | 200000 |
| NU | 0.3 |
| TENS-1 | 430 |
| TORS-1 | 250 |

| Solution option | Parameter |
|--|-----------|
| Number of scanned planes | 120 |
| Shear component description <0~MCCM, 1~LCM, 2~by normal line, 3~MC | 0 |
| Negative mean stress <0~zeroized, 1~used> | 0 |
| Only every x-th data-point taken from load history | 1 |

MCD
 WB96
 WB93_1
 WB93_2
 FINDLEYS_WB
 FINDLEYS_SR
 FINDLEYS_MAX
 DV
 SOCSHEAR
 MATAKE
 LM
 CS
 SWT_WB
 SWT_VMRED
 MCD91
 FINDLEYS

ID-name:

Description:

Method: Material:

Decomposition:

Elasto-plasticity:

Mean stress influence:

Influence of stress gradient:

Influence of technology:

Influence of surface quality:

Influence of size:

Influence of temperature:

Set another survive probability:

Cumulative rule:

| Material parameters | Value |
|---------------------|--------|
| E | 200000 |
| NU | 0.3 |
| TENS-1 | 430 |
| TORS-1 | 250 |

| Solution option | Parameter |
|---|-----------|
| Searched planes <0~BS, 1~globe, 2~random, 3~N only> | 1 |
| Number of scanned planes | 45 |
| Shear component description <0~MCCM, 1~LCM, 2~by normal line, 3~MC> | 0 |
| Optimize <1~yes, 0~no> | 1 |
| Negative mean stress <0~zeroized, 1~used> | 0 |
| Only every x-th data-point taken from load history | 1 |

MCD
 WB96
 WB93_1
 WB93_2
 FINDLEYS_WB
 FINDLEYS_SR
 FINDLEYS_MAX
 DV
 SOCSHEAR
MATAKE
 LM
 CS
 SWT_WB
 SWT_VMRED
 MCD91
 FINDLEYS

ID-name:

Description:

Method: Material:

Decomposition:

| Material parameters | Value |
|---------------------|--------|
| E | 200000 |
| NU | 0.3 |
| TENS-1 | 430 |
| TORS-1 | 250 |

Elasto-plasticity:

Mean stress influence:

Influence of stress gradient:

Influence of technology:

Influence of surface quality:

Influence of size:

Influence of temperature:

Set another survive probability:

Cumulative rule:

| Solution option | Parameter |
|--|-----------|
| Searched planes <0~BS, 1~globe, 2~random, 3~N only > | 1 |
| Number of scanned planes | 45 |
| Shear component description <0~MCCM, 1~LCM, 2~by normal line, 3~MC | 0 |
| Optimize <1~yes, 0~no > | 1 |
| Negative mean stress <0~zeroized, 1~used > | 0 |
| Only every x-th data-point taken from load history | 1 |

MCD
WB96
WB93_1
WB93_2
FINDLEYS_WB
FINDLEYS_SR
FINDLEYS_MAX
DV
SOCSHEAR
MATAKE
LM
CS
SWT_WB
SWT_VMRED
MCD91
FINDLEYCS

ID-name: SOCSHEAR

Description:

Method: Socie (shear v.) Material: 3

Decomposition: Rain-flow of resolved shear variable

Elasto-plasticity: No

Mean stress influence: As in original formula

Influence of stress gradient: No

Influence of technology: No

Influence of surface quality: No

Influence of size: No

Influence of temperature: No

Set another survive probability: No

Cumulative rule: Palmgren-Miner

| Material parameters | Value |
|---------------------|--------|
| E | 200000 |
| NU | 0.3 |
| SIG_YLD | 550 |
| TAU_F | 900 |
| GAMMA_F | 0.42 |
| EXP_B | -0.139 |
| EXP_C | -0.498 |
| C_SOCS | 1 |
| G | 80000 |

| Solution option | Parameter |
|---|-----------|
| Searched planes <0~BS, 1~globe, 2~random, 3~N only> | 1 |
| Number of scanned planes | 45 |
| Shear component description <0~MCCM, 1~LCM, 2~by normal line, 3~MC0 | 0 |
| Optimize <1~yes, 0~no> | 1 |

| Solution variable | Value |
|---|-------|
| Minimum damage | 1E-20 |
| Weight of non-closed half-cycles | 0.5 |
| Size of too small cycles (to be erased) | 0 |

Help Save New Remove

Skip Copy Close

MCD
 WB96
 WB93_1
 WB93_2
 FINDLEYS_WB
 FINDLEYS_SR
 FINDLEYS_MAX
 DV
 SOCSHEAR
 MATAKE
 LM
 CS
SWT_WB
 SWT_VMRED
 MCD91
 FINDLEYS

ID-name:

Description:

Method: Material:

Decomposition:

Elasto-plasticity:

Mean stress influence:

Influence of stress gradient:

Influence of technology:

Influence of surface quality:

Influence of size:

Influence of temperature:

Set another survive probability:

Cumulative rule:

| Material parameters | Value |
|---------------------|--------|
| E | 200000 |
| NU | 0.3 |
| SIG_F | 1700 |
| EPS_F | 0.33 |
| EXP_B | -0.139 |
| EXP_C | -0.498 |
| K' | 2200 |
| N' | 0.272 |

| Solution option | Parameter |
|--|-----------|
| Negative mean stress <0~zeroized, 1~used> | 0 |
| CP set <0~on each cycle, 1~on whole load history> | 1 |
| Only every x-th data-point taken from load history | 1 |

| Solution variable | Value |
|----------------------------------|-------|
| Minimum damage | 1E-20 |
| Weight of non-closed half-cycles | 0.5 |

Help Save New Remove
 Skip Copy Close

MCD
 WB96
 WB93_1
 WB93_2
 FINDLEYS_WB
 FINDLEYS_SR
 FINDLEYS_MAX
 DV
 SOCSHEAR
 MATAKE
 LM
 CS
 SWT_WB
SWT_VMRED
 MCD91
 FINDLEYS

ID-name:

Description:

Method: Material:

Decomposition:

Elasto-plasticity:

Mean stress influence:

Influence of stress gradient:

Influence of technology:

Influence of surface quality:

Influence of size:

Influence of temperature:

Set another survive probability:

Cumulative rule:

| Material parameters | Value |
|---------------------|--------|
| E | 200000 |
| NU | 0.3 |
| SIG_F | 1700 |
| EPS_F | 0.33 |
| EXP_B | -0.139 |
| EXP_C | -0.498 |
| K' | 2200 |
| N' | 0.272 |

| Solution option | Parameter |
|---|-----------|
| Negative mean stress <0~zeroized, 1~used> | 0 |
| Only every x-th data-point taken from load history | 1 |
| Close non-closed cycles in second run <1~yes, 0~no> | 1 |

| Solution variable | Value |
|---|-------|
| Minimum damage | 1E-20 |
| Weight of non-closed half-cycles | 0.5 |
| Size of too small cycles (to be erased) | 0 |

MCD
 WB96
 WB93_1
 WB93_2
 FINDLEYS_WB
 FINDLEYS_SR
 FINDLEYS_MAX
 DV
 SOCSHEAR
 MATAKE
 LM
 CS
 SWT_WB
 SWT_VMRED
 MCD91
FINDLEYS

ID-name:

Description:

Method: Material:

Decomposition:

Elasto-plasticity:

Mean stress influence:

Influence of stress gradient:

Influence of technology:

Influence of surface quality:

Influence of size:

Influence of temperature:

Set another survive probability:

Cumulative rule:

| Material parameters | Value |
|---------------------|--------|
| E | 200000 |
| NU | 0.3 |
| TENS-1 | 430 |
| TORS-1 | 250 |

| Solution option | Parameter |
|---|-----------|
| Searched planes <0~BS, 1~globe, 2~random, 3~N only> | 1 |
| Number of scanned planes | 45 |
| Shear component description <0~MCCM, 1~LCM, 2~by normal line, 3~MC> | 0 |
| Optimize <1~yes, 0~no> | 1 |
| Negative mean stress <0~zeroized, 1~used> | 0 |
| Only every x-th data-point taken from load history | 1 |

Help Save New Remove
 Skip Copy Close

C. Stress Time History Case 3 L3-L4

Time history computed at node experiencing most damage (according to Pragtic).

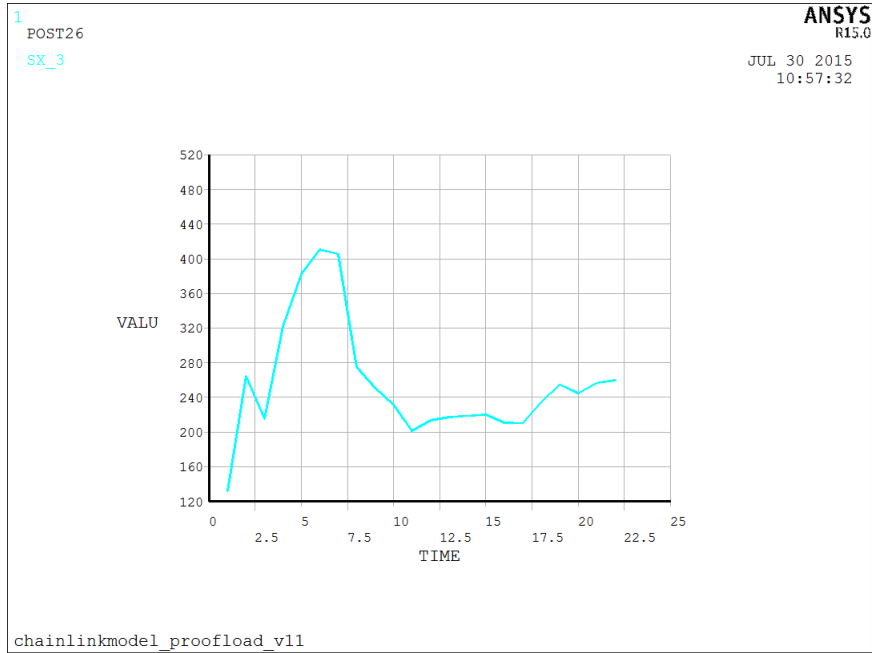


Figure C.1: Location 3; stress in X-direction

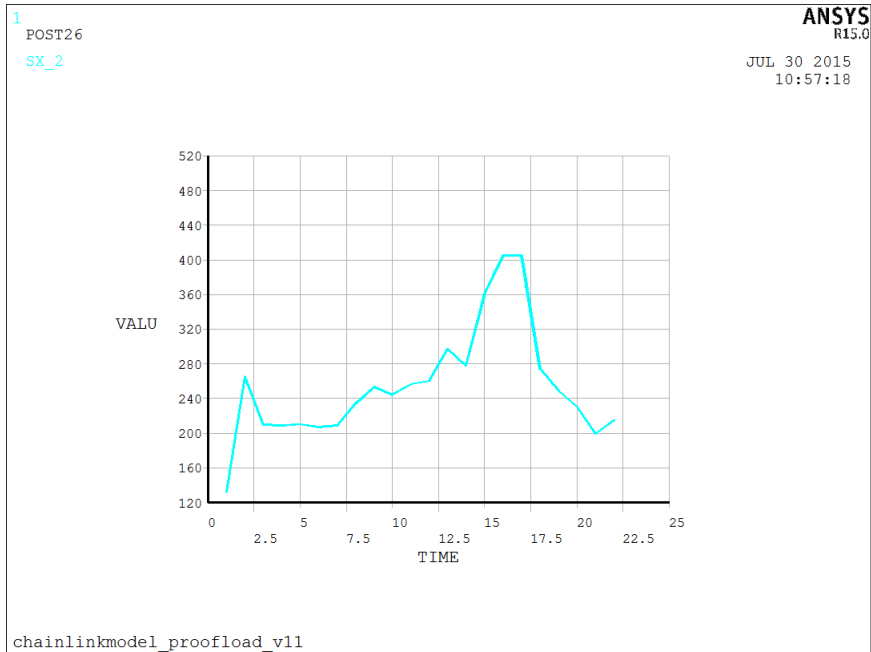


Figure C.2: Location 4; stress in X-direction

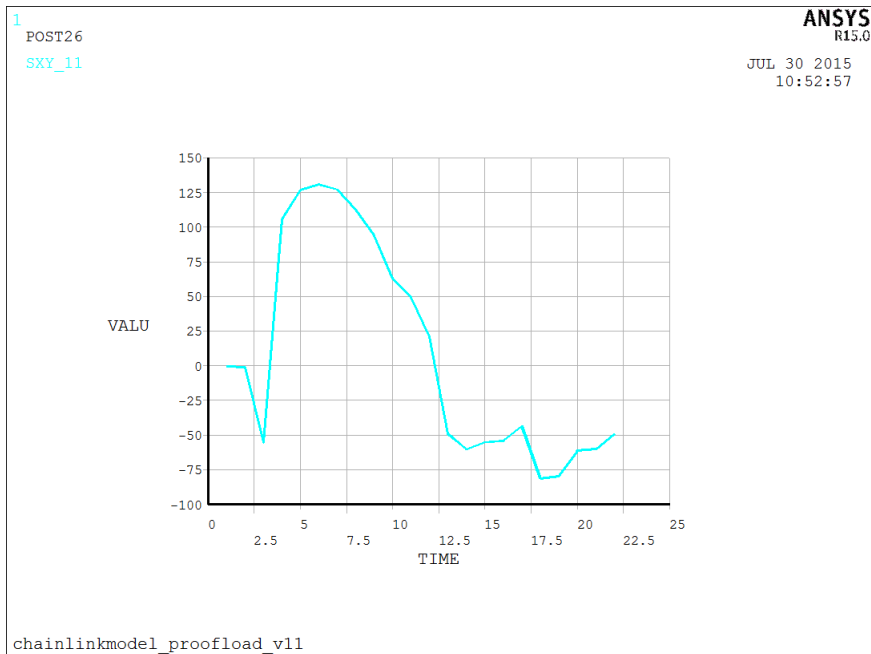


Figure C.3: Location 3; XY shear stress

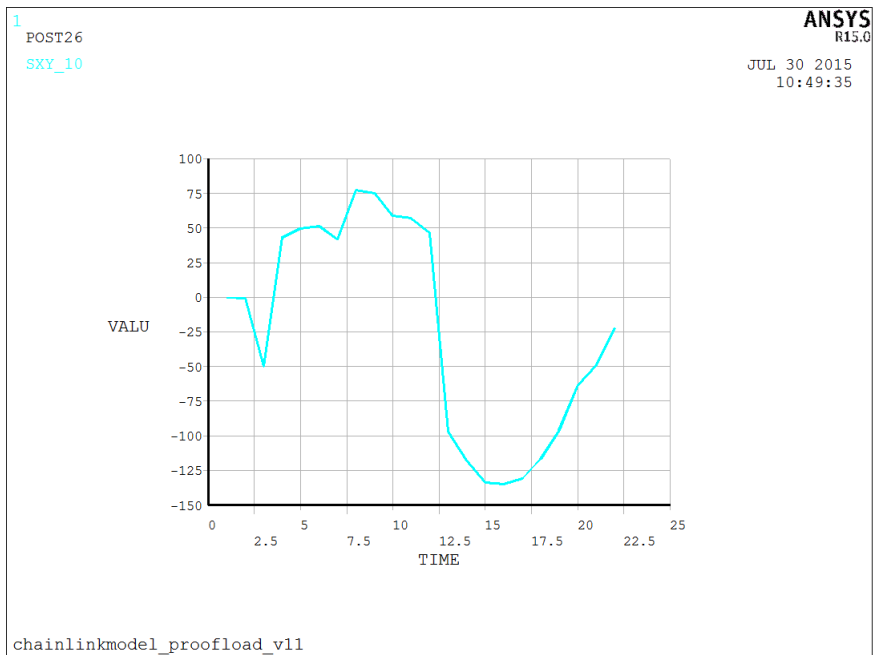


Figure C.4: Location 4; XY shear stress

Bibliography

- [Anes et al., 2014] Anes, V., Reis, L., and de Freitas, M. (2014). New cycle counting method for multiaxial fatigue. *International Journal of Fatigue*, 67:78–94.
- [Ansys, 2015] Ansys (2015). Ansys help. Technical report.
- [Bannantine and Socie, 1991] Bannantine, J. and Socie, D. (1991). A variable amplitude multiaxial fatigue life prediction method. *Fatigue under biaxial and multiaxial loading*, ESIS Publication 10:767–778.
- [Brown and Wang, 1996] Brown, M. and Wang, C. (1996). Life prediction techniques for variable amplitude multiaxial fatigue - part 1: Theories. *Fatigue and Fracture of Engineering materials and structures*, 118:367–370.
- [BV, 2014] BV (2014). Fatigue of top chain of mooring lines due to in-plane and out-of-plane bendings. Technical report, Burea Veritas Marine and Offshore Division.
- [Carpinteri and Spagnoli, 2003] Carpinteri, A. and Spagnoli, A. (2003). Multiaxial high-cycle fatigue criterion for hard metals. *Institute of Materials and Machine Mechanics*.
- [Fatemi,] Fatemi, A. Multiaxial fatigue. Lecture slides, University of Toledo.
- [Fatemi and Socie, 1988] Fatemi, A. and Socie, D. (1988). A critical plane approach to multiaxial fatigue damage including out-of-phase loading. *Fatigue and Fracture of Engineering materials and structures*, 11-3:149–166.
- [Fernandez, 2008] Fernandez, J. (2008). Reliability of mooring chains. Technical report, Offshore Unit Vicinay Cadenas, S.A.
- [Frunza and Diaconescu, 2006] Frunza, G. and Diaconescu, E. (2006). Hysteresis and mechanical fatigue. *The annals of university “Dunarea de Jos” of Galati*, VIII:61–66.
- [Golisz, 2015] Golisz, T. (2015). Chain link opb fatigue analysis. Technical report, London Marine Consultants.
- [Griffith, 1920] Griffith, A. (1920). The phenomena of rupture and flow in solids. *Royal Society*, CCXXI-A587.
- [Ince and Glinka, 2011] Ince, A. and Glinka, G. (2011). A modification of morrow and smith-watson-topper mean stress correction models. *Fatigue & Fracture of Engineering Materials & Structures*, 34:854–867.

- [Jean et al., 2005] Jean, P., Goessens, K., and L’Hostis, D. (2005). Failure of chains by bending on deepwater mooring systems. In *Offshore Technology Conference*, volume OTC17238.
- [Karolczuk and Macha, NOWN] Karolczuk, A. and Macha, E. (UNKNOWN). Fatigue fracture planes and the critical plane orientations in multiaxial fatigue failure criteria. Unsure about official publishing.
- [Liu and Mahadevan, 2007] Liu, Y. and Mahadevan, S. (2007). A unified multiaxial fatigue damage model for isotropic and anisotropic materials. *International Journal of Fatigue*, 29:347–359.
- [Liu et al., 2006] Liu, Y., Stratman, B., and Mahadevan, S. (2006). Fatigue crack initiation life prediction of railroad wheels. *International Journal of Fatigue*, 28:747–756.
- [Matsuishi and Endo, 1968] Matsuishi, M. and Endo, T. (1968). Fatigue of metals subjected to varying stress. *Japanese Society of Mechanical Engineering*.
- [McDiarmid, 1994] McDiarmid, D. (1994). A shear-stress based critical-plane criterion of multiaxial fatigue failure for design and life prediction. *Fatigue and Fracture of Engineering materials and structures*, 17-12:1475–1485.
- [McKeighan and Ranganathan, 2005] McKeighan and Ranganathan (2005). *Fatigue Testing and Analysis under variable amplitude loading conditions*. ASTM, Conshohocken, PA, U.S.A.
- [Meggiolaro and de Castro, 2012a] Meggiolaro, M. and de Castro, J. T. P. (2012a). An improved multiaxial rainflow algorithm for non-proportional stress or strain histories - part i: Enclosing surface methods. *International Journal of Fatigue*, 42:217–226.
- [Meggiolaro and de Castro, 2012b] Meggiolaro, M. and de Castro, J. T. P. (2012b). An improved multiaxial rainflow algorithm for non-proportional stress or strain histories - part ii: The modified wang-brown method. *International Journal of Fatigue*, 42:194–206.
- [Mikhailov and Namestnikova, 2001] Mikhailov, S. and Namestnikova, I. (2001). Concept of normalised equivalent stress functionals for cyclic fatigue. *Preprint PP/MAT/SEM/0102-005, Glasgow Caledonian University*.
- [Papadopoulos, 1997] Papadopoulos, I. (1997). A comparative study of multiaxial high-cycle fatigue. *International Journal of Fatigue*, 19-3:219–235.
- [Papuga, 2005] Papuga, J. (2005). *Mapping of Fatigue Damages - Program Shell of FE-Calculation*. PhD thesis, Czech Technical University, Technická 4, 166 07 Prague 6, Czech Republic.
- [Papuga, 2007] Papuga, J. (2007). Pragtic helpfile.
- [Paris, 1961] Paris, P. (1961). A rational analytic theory of fatigue. *The Trend in Engineering*, pages 9–14.

- [Rankine, 1842] Rankine, W. (1842). On the causes of the unexpected breakage of the journals of railway axles, and on the means of preventing such accidents by observing the law of continuity in their construction. *Institution of Civil Engineers Minutes of Proceedings*, pages 105–108.
- [Rychlik, 1987] Rychlik, I. (1987). A new definition of the rainflow cycle counting method. *International Journal of Fatigue*, 9-2:119–121.
- [Smith et al., 1970] Smith, R., Watson, P., and Topper, T. (1970). A stress-strain parameter for the fatigue of metals. *Journal of Materials*, 5-4:767–778.
- [Socie, 1982] Socie, D. (1982). Simple rainflow counting algorithms. *International Journal of Fatigue*, 4-1:31–40.
- [Socie and Marquis, 2000] Socie, D. and Marquis, G. (2000). *Multiaxial Fatigue*. SAE, Inc., Warrendale, PA, U.S.A.
- [Sonsino, 1997] Sonsino, C. (1997). Overview of the state of the art on multiaxial fatigue of welds. In *5th Int. Conference on Biaxial/Multiaxial Fatigue and Fracture*, Cracow, Poland.
- [Susmel et al., 2005] Susmel, L., Tovo, R., and Lazzarin, P. (2005). The mean stress effect on the high-cycle fatigue strength from a multiaxial fatigue point of view. *International Journal of Fatigue*, pages 928–943.
- [Čačko, 1999] Čačko, J. (1999). Modelling of a fatigue cumulative damage under random loading conditions. Unsure about official publishing.